ToF-SIMS—An Overview

Article

1 author:

John C Vickerman
The University of Manchester
305 PUBLICATIONS **11,157** CITATIONS

SEE PROFILE

1 ToF-SIMS—An Overview

John C. Vickerman
Surface Analysis Research Centre, Department of Chemistry, UMIST, Manchester, UK

1.1 Static SIMS—the essence

Secondary ion mass spectrometry, SIMS, is the mass spectrometry of ionised particles which are emitted when a surface is bombarded by energetic primary particles, usually ions (for example, Ar^+, Ga^+, Cs^+). The emitted (sputtered) "secondary" particles will be electrons; neutrals species atoms or molecules; atomic and cluster ions. The vast majority of species emitted are neutral but it is the secondary ions that are detected and analysed by a mass spectrometer. It is this process which provides a mass spectrum of a surface and enables a detailed chemical analysis of a surface or solid to be performed.

Time-of-flight SIMS (ToF-SIMS) is the dominant experimental variant of *static SIMS* that emerged as a technique of potential importance in surface science as a consequence of the work of Benninghoven and his group in Münster in the late 1960s (see Chapter 2). Conceptually the process is very simple: Figure 1 (see also Figure 1 in Chapter 2). When a high energy (between 1 and 25 keV) beam of ions or neutrals bombards a surface, the particle energy is transferred to the atoms of the solid by billiard-ball-type collisional process. A "cascade" of collisions occurs between the atoms in the solid; some collisions return to the surface and result in the emission of atoms and atom clusters, some of which are ionised in the course of leaving the surface. While the technique is apparently destructive, the essence of the *static* mode is to use an extremely low dose of primary ions (never more than 10^{13} ions cm^{-2}), such that within the time scale of the experi-

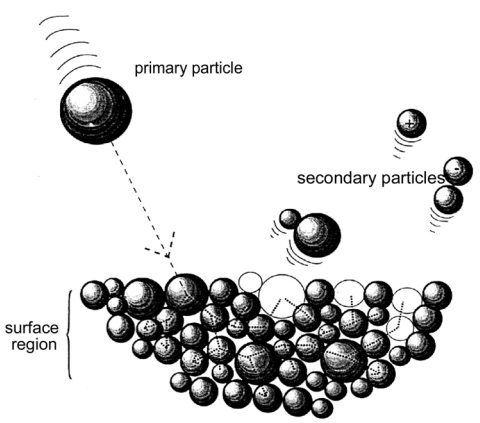

Figure 1. A schematic diagram of the SIMS process.

ment very much less than 1% of the top surface layer of atoms or molecules receives an ion impact. Under these conditions on a random impact basis no spot on the surface should receive more than one primary ion strike. The species generated arise from an area no greater than 10 nm^2 and are remote from the next point of analytical impact. The vast majority of the surface will be unaware of the removal of these species or any local effects as a consequence of the sputtering event. Thus the spectral information arises from a surface which is, for all practical purposes, undamaged. The final collision resulting in secondary particle emission is of low energy (~20 eV); over 95% of the secondary particles originate from the top two layers of the solid. Thus the possibility of a soft ionisation mass spectrometry of the surface layer emerges. There is now a very large body of evidence from a wide range of chemistries, from model single crystal adsorbate systems[1] to complex polymer-based materials (see Chapters 7, 18–20), which amply demonstrates that when using *static* analysis conditions there is a clear relationship between SSIMS spectra and surface chemistry. Part of the positive-ion spectrum of the surface of a film of poly(ethylene terephthalate) illustrates this well, Figure 2. It is distinctive and analytically definitive for PET. The peaks at 191/193 are the [M – H] and [M + H] ions from the PET monomer, the other major peaks at 149 and 105/104 are fragments of the monomer ion and are analytically helpful in defining the structure.

1.2 Basic experimental parameters

The potential shown by this simple example arise from a process which appears to be rather violent. Indeed in the early days of its exploitation there were many in the surface physics community who suggested that "no good" would come of this technique. It was altogether too violent and crude. Far better to irradiate your samples with electrons! What is known about the processes underlying static SIMS?

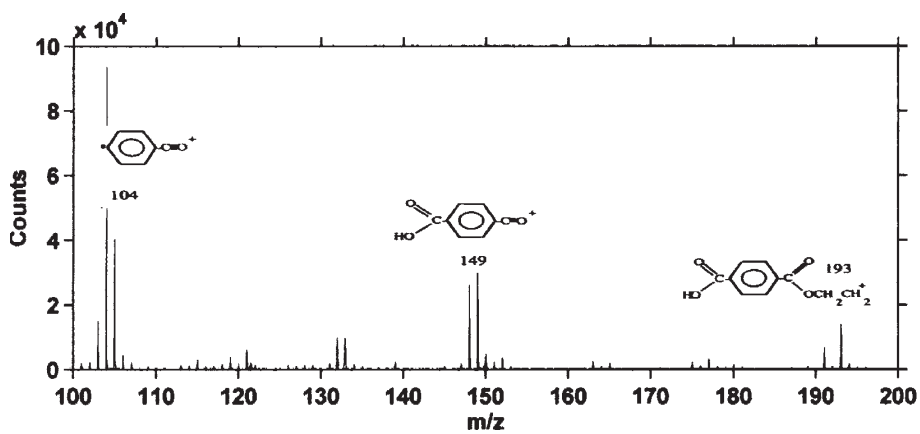

Figure 2. Part of the positive-ion spectrum of poly(ethylene terephthalate).

1.2.1 The basic equation

A more extensive introduction to the phenomenology of sputtering and secondary ion emission can be found elsewhere.[2–5] SSIMS is concerned with the analysis of secondary *ions*. Ionisation occurs at, or close to, emission of the particles from the surface with the consequence that the matrix participates in the electronic processes involved. This means that the yield of secondary ions is strongly influenced by the electronic state of the material being analysed with consequent complications for quantitative analysis. The basic SIMS equation is

$$I_m = I_p Y_m \alpha^+ \theta_m \eta \tag{1}$$

where I_m is the secondary ion current of species m, I_p is the primary particle flux, Y_m is the sputter yield, α^+ is the ionisation probability to *positive ions,* θ_m is the fractional concentration of the chemistry m in the surface layer and η is the transmission of the analysis system.

1.2.1.1 Sputtering

The two fundamental parameters are Y_m and α^+. Y_m is the total yield of sputtered particles of species m, neutral and ionic, per primary particle impact. It increases linearly with primary flux. It also increases with primary particle mass, charge and energy, although not linearly. Figure 3 shows the variation of Y for aluminium. The crystallinity and topography of the bombarded material will also affect the yield. The threshold for sputtering occurs at about 20 to 40 eV primary particle energy and y tends to maximise with energy at around between 5 and 50 keV. Beyond this energy yield drops away as the primary beam penetrates deeper into the solid and less energy returns to the surface

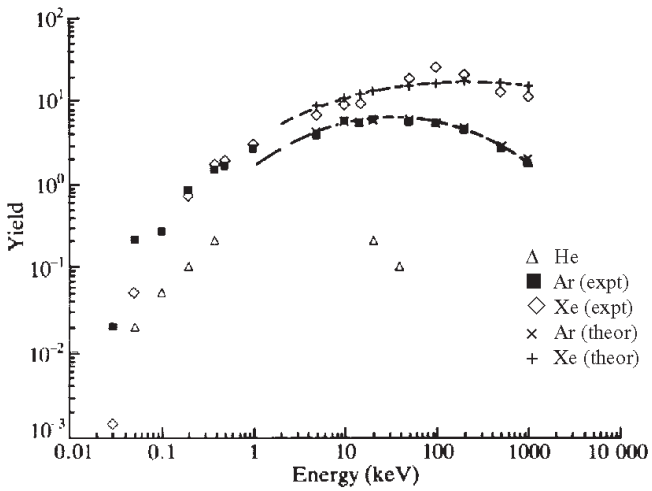

Figure 3. Variation of the sputter yield from aluminium metal as a function of primary beam type and energy. The figure summarises data from a wide range of sources.

region. For amorphous or polycrystalline materials sputter yield increases monotonically with increasing incident angle relative to the surface normal to a maximum at about 60 to 80°. The angular distribution of sputtered material tends to have a cosine distribution around the angle of reflection of the primary beam. Generally, the larger the mass of the bombarding particle, the closer to surface the energy will be deposited and hence the greater will be the yield. At a given bombardment energy the sputter yield for elements varies by a factor of three to five through the periodic table.

Sputtering is a damaging process, consequently it is more difficult to measure sputter rates for covalent organic materials (see Hagenhoff, Chapter 11, Figure 1). The yield of elemental carbon could be measured, but in static SIMS we are more interested in using the technique to detect and measure chemical structure. Sputtering of organic materials results in the removal of elements, structural fragments and molecular species. The loss of any of these entities from the surface will destroy the chemical structure within the area from which it is removed. If the material is molecular, every molecule impacted will be effectively destroyed, whether all the molecule or only a small piece of the molecule is removed. If the material is a polymer, then that part of the monomer unit impacted will be destroyed. Thus instead of sputter rate the concept of *damage cross-section*, σ, has been found to be more useful. The loss of structurally-significant species from the SSIMS spectrum as a function of bombardment time is taken to be a measure of the increasing damage. Clearly this measurement is in contrast to sputter yield measurements where the material removed from the surface is collected. The *damage cross-section,* σ, is related to the secondary ion intensity for chemistry *m* by the equation:

$$I_m = I_{mo} \exp(-\sigma I_p) \tag{2}$$

Benninghoven *et al*. obtained damage cross-sections of around 10^{-14} cm^{-2} for amino acid and other small molecules on metal substrates.[6] In the case of polymers there is a decay in the intensity of characteristic fragment ions. It is usually observed that the larger the fragment, the greater the rate of damage. However, since removal of backbone parts of the polymer will require more than one scission point, there is frequently a rise in intensity of these fragments, before they start to decay.[7] The *damage cross-section* can be thought of as the average area per incident particle from which the emission of the particular species being analysed is excluded. 10^{-14} cm^2 is an area 10 Å square which is about the size of the fragments detected. As for elemental sputtering, secondary ion yields and damage cross-sections for organic materials increase with primary ion mass and energy and increasing angle of incidence away from normal.[8] It is also observed that there is an increased relative yield of high mass fragments and molecular species.[9,10] In recent years there has been increasing interest in the use of polyatomic primary ions, SF_5^+, C_6H_{12}, Au_n^+, C_{60}^+. These ions have been shown to deliver significantly higher ion yields, particularly of high mass species, see section 1.7.2 and Stipdonk's Chapter 12.

Atoms, molecules and molecular fragments sputtered from the surface of solids are emitted with a range of kinetic energies. The kinetic energy distribution is influenced indirectly by the primary ion energy, angle of incidence and atomicity which will deter-

mine the nature of the collision cascades in the material. However, of more direct influence will be the binding of the species in the surface, the number of bonds to be broken, the degree to which internal energy can be stored by the emitted species. The kinetic energy distribution of an atomic secondary ion from a metal will generally be broad, typical of collisional sputtering, Figure 4(a), whereas that of cluster ions will be very much narrower because they can loose energy by fragmentation or storing it in vibrations and rotations, Figure 4(b). The kinetic energy distributions of large molecular species from organic materials are usually very narrow. If such a species fragments as it leaves the surface, the resulting fragment may show a negative a negative tail in the distribution, Figure 4(c). Thus kinetic energy distributions can reveal a good deal about the mechanisms of the emission process. This is discussed in a great deal more detail by Delcorte in Chapter 7.

1.2.1.2 Ionisation

Secondary ion formation is strongly influenced by electron exchange processes between the departing species and the surface. Thus the electronic state of the surface is critical. The yields of elemental secondary ions can vary by several orders of magnitude across the periodic table, Figure 5, and are very dependent on the chemical state of the surface (the *matrix effect*). Thus the ion yield for a particular element will vary dramatically, for example, from a metal as compared to its oxide, Table 1. It can be seen that oxidation changes the elemental ion yields to differing extents resulting in significant complications when absolute quantitative data is required.

Secondary ion formation from organic materials can occur by a number of mechanisms. Ejection of an electron to form an odd electron ion $M^{\bullet+}$; polar molecules may undergo acid base reactions to form $[M + H]^+$ or $[M - H]^\pm$ ions; cationisation or anionisation of neutral molecules may occur. These processes are mainly relevant to molecular type species, low mass fragments also provide important information for chemical structure determination. Ionisation of these species probably occurs via a collision-induced mechanism due to direct interaction with the primary ion or energetic recoil atoms within the material. The exact locus of these ionisation processes is not known, but is likely in the emission region within or just above the surface. Matrix effects do influence secondary ion yields from organic materials, but they are generally not so marked as from inorganic systems. Ion yields from copolymers have been observed to be sensitive to identity of the components. Clearly cationisation will be favoured when suitable cations (Ag, K, H) are available in the matrix. This area is reviewed by Hagenhoff in Chapter 11.

1.2.2 Monolayer lifetime and the Static Limit

As indicated in the introduction *Static* conditions are those that maintain the integrity of the surface layer within the time-scale of the analytical experiment. This implies that a very low primary beam dose is used during analysis. The distinction between dynamic and static conditions can be understood by computing the lifetime, t_m, of the topmost atomic layer as a function of the primary beam flux at the sample surface.

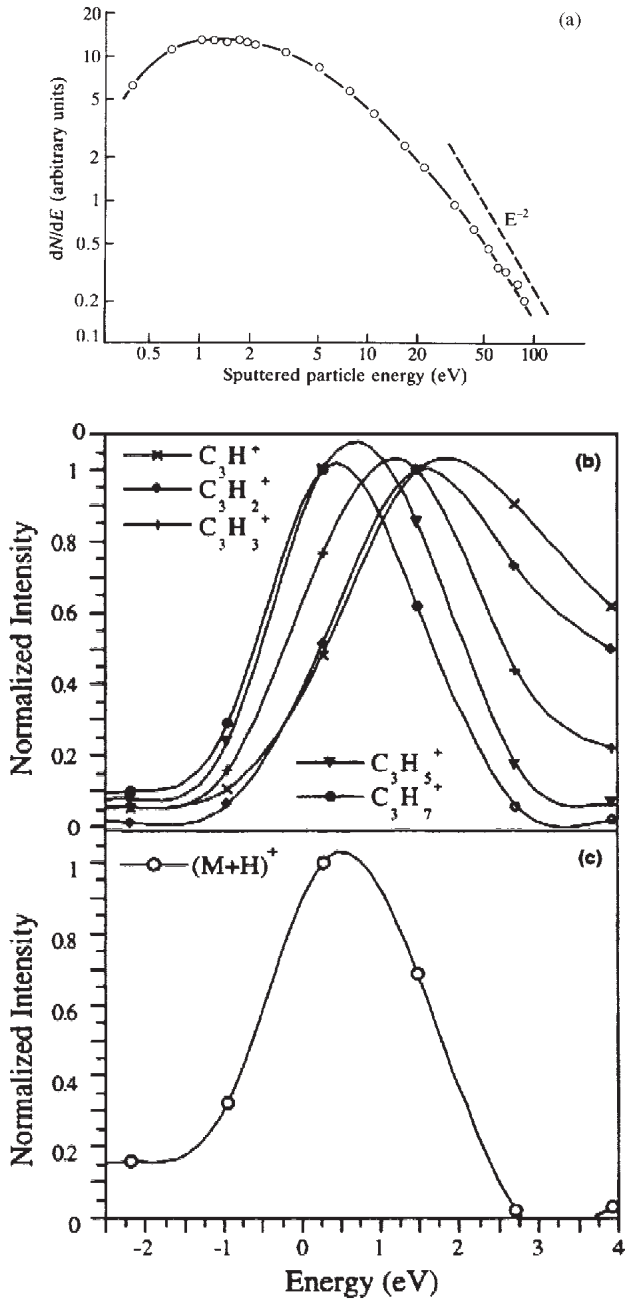

Figure 4. (a) The energy distribution of sputtered gold atoms due to the impact of 16 keV Ar^+ on polycrystalline gold, from *J. Nucl. Mater.* 76/77, 136 (1978). (b) and (c) kinetic energy distributions of positive-ion species sputtered from a layer of tricosenoic acid ($C_{22}H_{43}COOH$) on gold, from A. Delcorte and P. Bertrand, *Nucl. Instrum. Meth. Phys. Res. B* 115, 246 (1996).

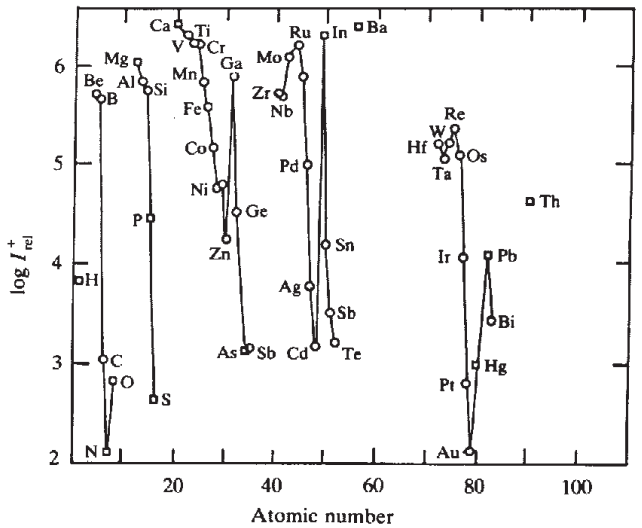

Figure 5. Variation of elemental positive secondary ion yield as a function of atomic number for bombardment by 13.5 keV O^-, from *Anal. Chem.* 49, 2023 (1977).

$$t_m = \frac{10^{15}}{I_p} \times \frac{A}{Y} \tag{3}$$

where A cm^2 of the surface (surface layer atom density of 10^{15} atoms cm^{-2}) is bombarded by a primary beam of flux density I_p particles cm^{-2} and the sputter yield is Y. Usually the primary beam flux is measured in Amps cm^{-2}. (1 Amp is equivalent to 6.2×10^{18} charged particles s^{-1}). Using this equation, assuming a sputter yield of 1, Table 2 has been assembled.

If an analysis requires say 20 minutes (1200 s) then static conditions can only be safely attained for primary beam currents of about 1 nA cm^{-2} or less. An alternative approach takes account of the fact that each impact physically influences an area of 10 nm^2 which implies 10^{13} impacts cm^{-2} to influence all the atoms in the surface. This is generally accepted as the static primary particle dose limit.

For dynamic SIMS, high elemental sensitivity and rapid erosion rates are required so high primary flux densities of 1 μA cm^{-2} or greater are desirable. The time to complete a depth profile will be of principal interest. Clearly the magnitude of Y is significant in these calculations. Whilst these are well known for a wide range of primary particle mass, energy and angle of incidence for metallic targets, the sputtering characteristics of organic and other molecular materials are not known in any real detail. However, it is known that a static limit of 10^{13} impacts cm^{-2} is probably too high for most organic materials. Early studies by a number of groups of ion beam induced effects on polymers demonstrated that damage can be detected even before 10^{12} impacts cm^{-2}.[11] Indeed *damage cross-sections* of 10^{-14} cm^{-2} imply that characteristic ion signal intensity will be reduced by 1 to 10% for a dose in the range of 10^{12} to 10^{13} ions cm^{-2}.

Table 1. Elemental positive secondary ion yield from a number of metals compared to the corresponding oxides.

Metal	Clean metals M^+ yield	Oxide M^+ yield
Mg	0.01	0.9
Al	0.007	0.7
Si	0.0084	0.58
Ti	0.0013	0.4
V	0.001	0.3
Cr	0.0012	1.2
Mn	0.0006	0.3
Fe	0.0015	0.35
Ni	0.0006	0.045
Cu	0.0003	0.007
Ge	0.0044	0.02
Sr	0.0002	0.16
Nb	0.0006	0.05
Mo	0.00065	0.4
Ba	0.0002	0.03
Ta	0.00007	0.02
W	0.00009	0.035

Table 2. The surface monolayer lifetime as a function of primary beam flux density.

I_p (A cm^{-2})	t_m (s)
10^{-5}	16
10^{-7}	1600
10^{-9}	1.6×10^5
10^{-11}	1.6×10^7

1.2.3 Surface charging

Many of the important technological materials requiring surface analysis are insulators. When an insulating sample is bombarded by a positive ion beam, the surface potential rises due to the input of positive charge and the emission of secondary electrons. The potential can rise very rapidly by several hundred volts in a few minutes, such that the kinetic energy of the emitted positive ions rises well beyond the acceptance window of the analyser.[12] The result is the loss of the SSIMS spectrum. An early and very successful solution to this problem for positive-ion quadrupole SIMS was to use a neutral atom beams (fast atom bombardment).[13] The need for pulsed primary beams in ToF-SIMS made this solution more difficult and there are now two linked solutions to this problem. The first, widely-used method, is to irradiate the sample surface with a beam of relatively low-energy electrons. The theory is that the electrons will be attracted to the region of positive charge on the surface and hence the surface potential will return to neutral. This usually works quite well for positive-ion SSIMS, however, for negative ion detection it is necessary to drive the surface potential negative in order for the negative ions to be released from the surface. This requires a higher flux of electrons, usually about ten times that of the ion flux. The balance is sometimes difficult to attain, particularly if the material is rough or of small dimensions, for example, fibres or granules. This approach is discussed in some detail by Gilmore in Chapter 10, but one disadvantage of this approach is that electron flooding can also give rise to sample degradation and electron stimulated ion emission. The alternative or linked solution is to either to place a metal grid in close electrical contact with the sample, or deposit the material as a thin film on silver. The use of thin, incomplete polymer films supported on specially treated silver foils is particularly advocated by some workers, see Hagenhoff, Chapter 11. Because the film is very thin, little charging occurs and this allows the SSIMS spectra to be acquired without any charge neutralisation. The possibility of electron beam induced degradation effects is then obviated. However, the spectra usually display considerable cationisation by the silver support. This can be helpful or not depending on the analytical requirements.

1.2.4 Evidence for the mechanism of secondary ion formation

The mechanism of secondary ion formation from organics is not fully understood. A range of experiments studied the process from different directions. Benninghoven *et al.* investigated the sputtering of organic molecules on metal substrates;[14] Briggs studied the characteristics of polymer sputtering from damage studies,[15] Leggett and Vickerman used MS/MS techniques to probe the mechanisms of fragment formation from polymers,[16] Delcorte and Bertrand studied the kinetic energy distributions of ions emitted from molecular and polymer materials.[17] From these various approaches a consensus has been reached as to the overall process involved. If the organic is a thin film supported on a metal substrate, close to the point of primary ion impact, high-energy events take place leading to the emission of atomic species and the fragmentation of the organic backbone. This will be followed by collision cascades in the metal substrate, the energy initially deposited by the primary particle falls off exponentially with successive collisions of

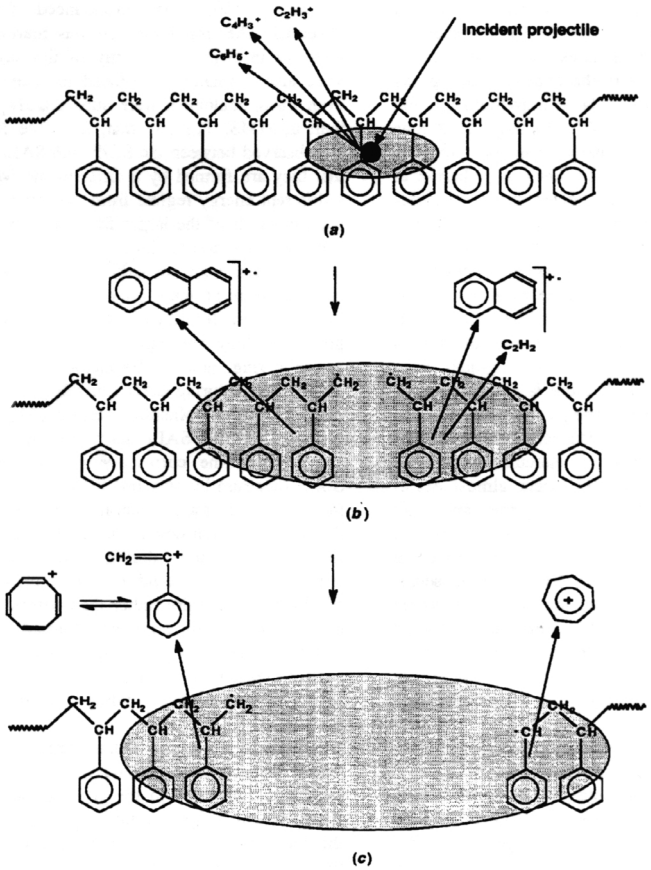

Figure 6. Model of sputtering of a polymer: (a) violent fragmentation in primary impact region; (b) unzipping to give large fragments in fingerprint region; (c) simple low-energy fragmentation in monomer region. [Following Leggett, in *The Static SIMS Library*, SurfaceSpectra Ltd, Manchester (1998).]

recoiling atoms, transferring decreasing amounts of energy to adsorbed molecules such that some desorb with significant amounts of internal energy and fragment, while other desorb without fragmentation.[18] The general concept of this model, formalised by Benninghoven, is probably valid for almost any form of material. The energy may not be transferred by the type of collision cascade envisaged in homogeneous elemental substrates. In the case of covalent molecular solids with directed bonds, energy will be transferred through vibrations. Thus in polymer material the events occurring as the energy spreads out from the impact point can be envisaged as shown in Figure 6.[19] The primary particle induces a physical scission in the polymer chain, which yields a macro-radical or ion. The primary ion energy is transformed into vibrational energy within the bonds of the molecule. As the energy is dissipated into the vibrational modes of the polymer, the poly-

mer is unzipped from point of fragmentation and successively larger lower energy fragments are emitted. Internal excitation leads to fragmentation via chemically determined pathways. Atomic species and small uncharacteristic organic fragments are thought to be emitted directly from the point of primary ion impact.

1.3 The ToF-SIMS Experiment

There are four main components for the static SIMS experiment: the primary particle source, the mass spectrometer and, since the secondary ions are emitted with a range of kinetic energies, an ion optical system which selects ions within a defined energy band compatible with the capability of the mass analyser and finally a detector. An electron source will also be required for charge compensation. The precise design can be tailored to optimise the performance for the particular analytical application envisaged. Chapters 3 and 4 provide a detailed discussion of the types of primary ion beam systems and mass analysers found on ToF-SIMS instruments. Figure 7 shows a schematic of the BioToF-SIMS instrument built by the UMIST and Penn State Groups.[20] A brief description of this system will serve to introduce the basic components of the experiment. This instrument has been particularly optimised for the analysis of molecules from biological materials. Whilst good mass resolution is required, the overriding requirement is high sensitivity and a good field of view. As with all analytical instruments a trade off has to be accepted.

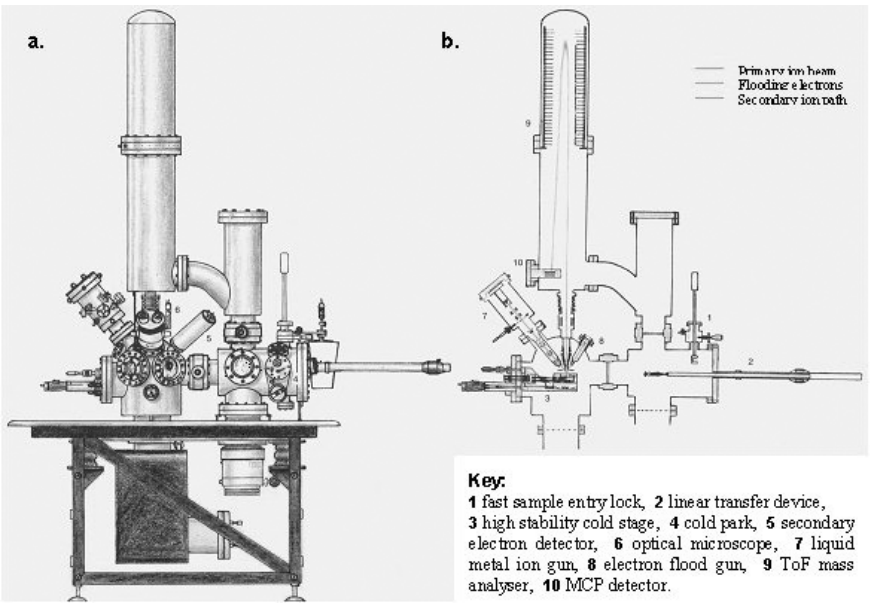

Figure 7. Schematic diagram of a ToF-SIMS instrument due to Steve Wong, *PhD Thesis,* UMIST, 2001.

The primary ion column[21] is mounted at 40° to the sample surface normal. It delivers a 25 keV $^{69}Ga^{+}$ beam from a mono-isotopic liquid gallium source. The beam can be pulsed with a pulse length varying from a ns up to several μs. The beam flux can be regulated from 60 pA to 50 nA by varying the beam apertures from 10 μm to 1 mm. This provides a flexible source which can be used as a high current source for rapid survey spectral acquisition or at low current as highly focussed beam for high spatial resolution analysis—down to sub-100 nm. A pulsed electron beam source with variable beam energy 10 to 1000 eV is provided for charge compensation. This can also be pulsed such that the electron pulses irradiate the sample between every primary ion pulse. The energy and flux of the beam can be independently adjusted.

Early static SIMS instruments used quadrupole mass analysers very successfully,[22] however, sensitivity was limited due to their low transmission and the fact they are scanning devices which throw away most of the information. In the 1980s there was a move to time-of-flight (ToF) analysers. Chait and Standing were probably the first to report results from a ToF-SIMS instrument in 1981,[23] using a linear flight tube, although there were a number of energy compensated ToF-SIMS in the pipeline then and soon after.[24] Their high transmission (>50%) and quasi-parallel detection mode delivered a better than 10^4 improvement in sensitivity, see Table 3. This, together with their good mass resolution ($m/\partial m$) > 4000), made them ideal static SIMS instruments. Time-of-flight mass spectrometry is conceptually the simplest means of mass separation. In ToF analysis pulses of secondary ions are accelerated to a given potential (3 to 8 keV) such that all ions possess the same kinetic energy; they are then allowed to drift through a field free space before striking the detector. According to the equation of kinetic energy, heavier masses travel more slowly through the "flight tube" and so the measured flight time, *t,* of ions of mass to charge ratio, *m/z,* accelerated by a potential *V* down a flight path of length *L* provides a simple means of mass analysis.

$$t = L\left(\frac{m}{2zV}\right)^{1/2} \tag{3}$$

The basic experimental requirement is for a precisely-pulsed primary ion source, a highly accurate computer clock, a drift tube and considerable computing power for data

Table 3. Comparison of mass analysers for SIMS.

Type	Resolution	Mass range	Transmission	Mass detection	Relative sensitivity
Quadrupole	10^2–10^3	$<10^3$	0.01–0.1	Sequential	1
Magnetic sector	10^4	$>10^4$	0.1–0.5	Sequential	10
Time-of-flight	$>10^3$	10^3–10^4	0.5–1.0	Parallel	10^4

acquisition. The flight times of all the ions to the detector are electronically measured and related to ion mass. Thus a mass spectrum of all the ions is generated from the flight time spectrum. Mass resolution is critically dependent upon the pulse length of the generated secondary ion pulse which should be precisely defined and very short. This in turn is dependent on the pulse length of primary beam which is typically in the order of nanoseconds. A detailed review of the theory of ToF analysers is presented by Schueler in Chapter 3.

The BioToF-SIMS utilises a two-stage reflectron analyser.[25] It has an effective path length of 3 m. It is inclined at 2.5° so that extracted secondary ions which travel up the optical axis, are separated from the reflected ions travelling back to the detector. The energy distribution of secondary ions will cause ions of the same mass to enter the drift tube with slightly different velocities and thus degrade the resolution in the final spectrum. This is compensated for using a reflectron or *ion mirror* which consists of a series of precisely spaced rings to which is applied a gradually increasing retarding field. The more energetic ions will penetrate further into the mirror before they are reflected, whilst the less energetic ions will take a slightly shorter path. When tuned correctly, all ions of the same mass will arrive at the detector at the same time, despite their small energy differences when leaving the sample surface.

The sensitivity advantages of ToF-SIMS suggested that *scanning* or *imaging* ToF-SIMS would in principle enable sub-μm molecular ion imaging. However, the critical parameter now becomes the secondary ion yield per pixel and in practise spatial resolution is limited by the number of molecules in a pixel area and the yields of molecular secondary ions from the material being studied. Such yields tend to be around 10^{-3} via the SIMS process. The only way to increase the yield and hence the ultimate spatial resolution is to post-ionise the vast number of neutral molecules in the sputtered plume. This instrument has therefore been constructed to enable laser post-ionisation of the sputtered neutrals to be easily accomplished (see section 1.7 and Chapters 13 to 15).

After the primary ions hit the sample the secondary ions are accelerated from the surface to the ToF analyser by a 2.5 keV field into the secondary ion optics, Figure 8, which is designed to work efficiently in both SSIMS and laser post-ionisation mode. It consists of a large bore, high transmission two-element lens. Both elements may be independently controlled which allows greater freedom when optimising the trade off between field of view, transmission and mass resolution. A large extraction region has been built into this instrument for two related reasons. First, to accommodate the facility to photo-ionise emitted neutrals (which compose over 95% of the emitted secondary species) using laser beams and, second, to increase the field of view or acceptance angle of the spectrometer. The consequence is that the extraction field is only 250 V mm^{-1} compared to 800 V mm^{-1} found in other instruments. The resulting large field of view will reduce the field distortions around rough samples and ensure that the voltage difference between the top and the bottom of the photo-ionising laser field is reduced, thus minimising any resulting reduction in mass resolution. The secondary ions are detected by a chevron type multichannel plate (MCP) consisting of a matched pair of 40 mm active diameter

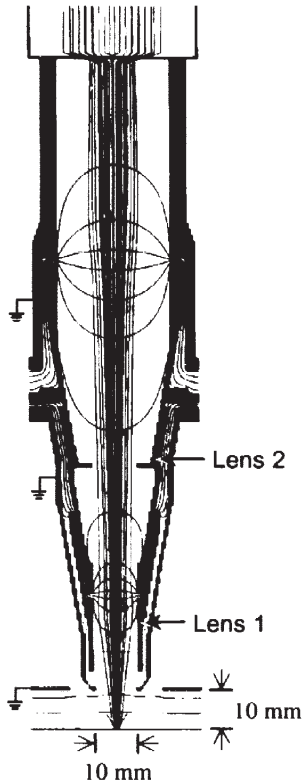

Figure 8. Schematic diagram of the extraction lens on the BioToFSIMS instrument showing the SIMION simulation of the extraction fields and the path taken by extracted secondary ions, Steve Wong, *PhD Thesis,* UMIST.

Galileo extended dynamic range microchannel plates. The ion detection efficiency of MCPs are strongly affected by secondary ion energy, mass and composition. For example, a large molecular species of mass 10,000 Da would require 130 keV collision to emit secondary electrons kinetically at the detector, so post-acceleration is required for high mass detection. A 25 keV post-accelerating detector is installed to improve the detection capability of the detector. Secondary events can be registered as either analogue or digital events. For static SIMS a time to digital converter (TDC) is generally employed, capable of high count rates and time resolution. For laser post-ionisation the primary ion pulse length has to be longer, consequently the count rates can be much larger which could saturate the TDC, consequently a transient digitiser is used.

This instrument is being developed to function as a chemical microscope for the analysis of biological samples, so the sample manipulation system is designed for rapid insertion of cold samples mounted on small copper blocks via a very low volume insertion lock. A cold parking stage in the preparation chamber allows samples to be stored

until analysis. There is also the facility for samples to be freeze-fractured. Samples can then be moved on a magnetically-operated transfer device to the analysis stage. The samples on their copper sample blocks are inserted into the high stability stage. The sample temperature can be controlled between 100 K and 400 K. The sample position can be precisely set in the x, y and z axes.

The effective and reproducible operation of a ToF-SIMS instrument requires very careful attention to sample preparation and instrumental parameters. These two areas are considered in some detail, respectively, by Reich in Chapter 5 and Gilmore in Chapter 10.

1.4 The theory of secondary ion generation

Ion formation in SIMS is a complex phenomenon. Simplistically, the process can be divided into two components: the dynamical process by which atoms and multi-atomic clusters are desorbed and the ionisation process in which a fraction of these sputtered particles become charged. Clearly electronic factors are involved throughout the desorption event. A good deal of theoretical work has gone into understanding the sputtering process and it is very encouraging that theory is increasingly able to rationalise the experimental observations. However, as yet the ionisation process is less tractable. Here we briefly outline a few of the main approaches to date. Since we are mainly concerned with surface analysis we will only consider the ideas which seek to explain the static SIMS process.

1.4.1 Models of sputtering

The simplest approach to sputtering of single component solids regards the atoms as hard spheres which obey Newtonian mechanics. Sigmund's linear cascade theory[26] has been the most successful model of the sputtering process so far. Urbassek outlines the current state of this approach in Chapter 6. Sigmund's model assumes that sputtering occurs by particle bombardment at small incident particle current and fluence. This excludes the situations where there is extensive heating and damage of the target and are close to the criteria for static SIMS. However, he also classifies sputtering events into knock-on sputtering and electronic sputtering. In his theory he disregards electronic sputtering. This approximation may well be valid for high incident primary particle energies, but in the low-energy (few keV) region typically used in SSIMS, electronic interactions between incident particles and target atoms may not be negligible and the hard sphere model may not be appropriate. The theory is developed on the basis of elastic collisions between point particles. Particular predictive success has attended the linear cascade ideas. In this process the incident particle transfers its energy to the target atoms and thereby initiates a series of collision *cascades* between the atoms of the solid within about 30 Å of the surface. Some of these collisions return to the surface and cause the emission of sputtered particles, see Figure 1 earlier. When applied to medium- to high-energy particle bombardment of single component materials the data match the experimental results in terms of the dependence of yields on primary particle mass and energy rather well, see Figure 3. However, at lower energies collision energy may be exchanged over greater dis-

tances than envisaged in the point mass collision cross-section and in complex multi-component materials (for example, polymers) the transport of energy will not be isotropic but highly directional.

To understand the sputtering process from complex materials, whilst Sigmund's theory gives some background ideas a different approach is required. In this regard various molecular dynamics (MD) simulations (particularly those due to Garrison and Winograd) have been very helpful in understanding the process occurring at the low primary flux densities encountered in SSIMS studies of inorganic materials.[27] An ensemble of a few hundred to a few thousand atoms is selected to model a crystal with a surface plane with specified initial conditions of atomic mass, position and velocity. An atomic interaction potential function is devised to account for the bonding of the crystal. The sample is then bombarded by a number of primary particles of specified mass, velocity and angle of incidence. The classical (Hamiltonian) equations of motion are solved in a sequence of iterative steps and the motions of the target atoms are determined as a function of time from the initial impact. The interaction potential is crucial in influencing the accuracy of the simulation. It not only determines the motions of the target atoms within the collision cascade volume, it also influences the nature of any bonding interactions between emitted atoms as polyatomic species are emitted. The embedded-atom potential method (EAM) has been very effective. For example, in studies of Rh atom desorption from Rh(111) very good agreement has been obtained between the theoretical and experimental energy distributions.[28] Similarly, the sputter yields from silver surfaces of Ag dimers relative to atoms together with their energy distributions also give good agreement between theory and experiment.[29]

Static SIMS analysis has been most effectively applied to the analysis of organic materials. These multi-element materials with highly directional bonding are more challenging to model and linear cascade theory is not really an appropriate sputtering model. The primary collision energy is thought to be deposited into molecular vibrations such that energy is exchanged within the organic layers via vibrational excitation. As the collision cascade evolves, many-body potential energy functions are required to allow for interactions occurring among the substrate atoms, the substrate and adsorbate atoms and between the individual adsorbate atoms. An example is the sputtering of self-assembled monolayers of alkanthiolates on gold.[30] Using this approach "mass spectra" of the sputter yield following bombardment by 500 eV Ar have been obtained which although no account is taken of ionisation, are very similar to those obtained experimentally. By examining the MD emission sequences it is possible to obtain insights into the possible mechanisms of secondary particle formation. It is clear that intact molecules are emitted as a consequence of collision cascades emerging from below, sometimes attached to substrate atoms, Figure 9. Both experiment and MD models show that frequently such large species are emitted with significant amounts of internal energy that leads to unimolecular fragmentation above the surface.[31] However, smaller fragments can also be formed as a consequence of direct impact of the primary particle with the molecules at the surface. Thus the generation of an experimental spectrum can be rationalised.

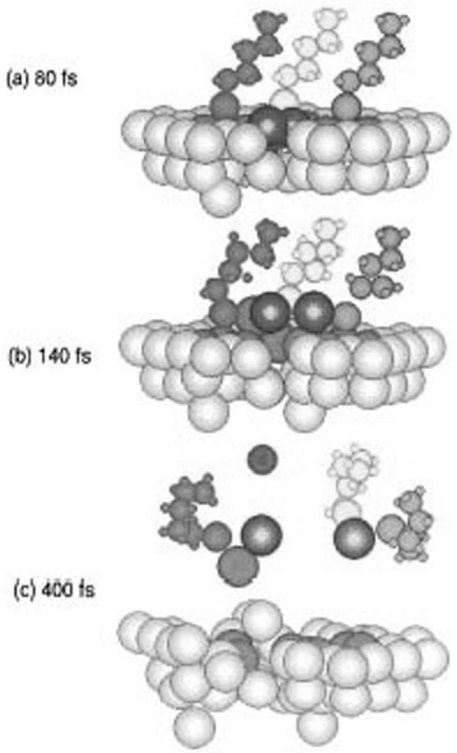

Figure 9. Two MD mechanisms for the sputter ejection of intact alkanethiolate molecules from threefold sites on a gold surface. One results in the emission of AuM_2 species, the other in the emission of Au_2M species. Both are seen in significant yield in the experimental negative ion spectrum. [Reproduced with permission from Liu *et al.*, *J. Phys. Chem. B* 103, 3195 (1999).]

As Garrison shows in more detail in Chapter 9 as the interaction potentials are developed to represent more realistically the forces within and between molecules in organic materials, these exciting calculations are beginning to reproduce the types of chemistry found in real organic layers. They are yielding simulations which have the feel of real SSIMS spectra, however, the whole problem of ionisation has yet to be addressed.

1.4.2 Ionisation

The fraction of sputtered particles which are in the ionised state is in fact very small. In most cases over 99% of the sputtered yield is neutral. Whether a sputtered particle escapes from the surface as an ion depends on the relative probabilities of ionisation and de-excitation as it passes through the near surface region. Hence the high dependence of ion yield on the electronic properties of the matrix (so called *matrix effect*). For metals the rapid electronic transitions (10^{14} to 10^{16} s^{-1}) make de-excitation a high probability during

the 10^{-13} s required for a sputtered particle to traverse the near surface region. The probability, P_a, of escape as an ion from a metal can be approximated by

$$P_a \approx 2/\pi \exp[-\pi(\varepsilon_a - \varepsilon_F)/\hbar\gamma_N v_1 \quad (4)$$

where ε_a and ε_F are the energies of the ionised state and the Fermi level, v_1 is the velocity of the emerging atom and γ_N^{-1} is the distance over which the level width decreases to 1/2.781 of the bulk value.

However, the need to develop an understanding of secondary ion emission from adsorbate and organic materials demands that we take account of the "molecular" covalent type of bonding and consider that ionisation may take place at emission and also by subsequent fragmentation of vibrationally-excited molecular units. Two helpful qualitative models suggested to describe the process of secondary ion generation from molecular solids are briefly described here.

1.4.2.1 Nascent ion molecule model

This model due to Gerhard and Plog[32] considered cluster ion formation primarily from oxide surfaces. It is suggested that the rapid electronic transition rates which occur in the surface region will neutralise any ions before they can escape. Secondary ions are thought to result as a consequence of dissociation of sputtered neutral molecular species some distance from the surface. In the terminology of the model, ions are formed by the non-adiabatic dissociation of *nascent ion molecules* (neutral molecules). For inorganic oxides most of the neutral molecules originate from direct emission of ion pairs such as MeO and keep their molecular character after leaving the surface. Only a few molecules have enough internal energy to dissociate into their constituents. The dissociation is considered to take place some distance from the surface where the electronic influence of the surface will be much smaller. The bond-breaking models which are used to explain emission from ionic materials consider the system solid-Me^+, whereas the nascent ion molecule considers the system $Me_xO_y^o$.

These ideas were further developed by Benninghoven into the Valence Model which predicted that the distribution of yields of these clusters (MO_x^+ and MO_y^-) from inorganic oxides would be dependent on the cation valance if it was assumed the oxygen anion maintained its charge as –2.[33] Empirically, this approach has had some success, however, it is highly doubtful that even before sputtering inorganic oxides can be regarded as purely ionic solids. Sanderson, many years ago, demonstrated that inorganic oxides have a large degree of covalency and the actual partial charge on each ion is a small fraction of the nominal ionic charge.[34] Further, it is highly unlikely that charge will be conserved when the bonds are broken during sputtering. A development of this model which makes no assumptions about the charge on oxygen takes this into account and demonstrates that indeed the static SIMS data suggested partial charges on the cations and anions which deviate from the pure ionic values.[35] It is clear that while the idea that the emission and fragmentation of nascent ion molecules is a major process is attractively straight-forward, and to first order may deliver helpful results, nevertheless the detail may

be misleading if accepted at face-value. The mechanism of formation of secondary ions from inorganic materials is considered in more detail by Adriens in Chapter 8.

1.4.2.2 The desorption ionisation model

Cooks and Busch introduced the concept that vibrational excitation may be important in understanding the emission of cluster or molecular ions from organic materials.[36] This model also emphasises that the processes of desorption and ionisation can be considered separately and however we understand the initial excitation process, the energy is transformed into thermal/vibrational motion as far as the molecules are concerned. A wide variety of ion emission processes are possible. Again there is the idea that some preformed ions may be directly emitted. These are species which exist as ions within the material prior to bombardment and no ionisation step occurs. It is suggested that neutral molecules are desorbed in high yield, but to be detected must undergo an ionisation process such as cationisation. To generate other ions, the model suggests that desorption is followed by two types of chemical reaction: (i) in the selvedge or top surface layers fast ion/molecule reactions or electron ionisation can occur; (ii) in free vacuum unimolecular fragmentation may occur, governed by the internal energy of the parent ion giving rise to fragment ions.

According to these ideas the desorption event is of relatively low energy. The linear cascade ideas are not wholly appropriate when considering molecular solids. It is more helpful to think of energy being transferred to the vibrational modes of the molecule thus leading to fragmentation and ionisation. This is consistent with the observation that SSIMS is a relatively soft-ionisation phenomenon: for many materials, there is relatively little low mass fragmentation and large yields of molecular ions are observed.

1.5 Static SIMS as a surface mass spectrometry

Whilst these qualitative models help us to understand what might happen during sputtering and ionisation of molecular surface species, as yet they do not provide any *a priori* grounds for *expecting* a direct relationship between SSIMS spectra and surface chemical structure, nor do they help to contribute towards predictive rules for the interpretation of spectra. The sceptics have repeatedly pointed to the perceived high-energy nature of the sputtering process. As indicated above, the data generated suggest otherwise. However, the mechanism of sputtering is different from other forms of mass spectrometry so progress in the application of static SIMS as a method of surface chemical analysis has had to rely on a pragmatic experimental approach. The initial strategy has been to investigate surface chemistry which has been well characterised by other techniques and to assess the SSIMS data in the light of that knowledge. Confidence has then grown that SSIMS is indeed a surface mass spectrometry generating valuable chemical structure information and as the experience of the technique has developed so the rules of spectral interpretation are being defined. As Benninghoven describes in Chapter 2, his studies on oxide surfaces provided early evidence of the sensitivity of static SIMS to

chemical structure. In the period 1976 to 1985 studies at UMIST demonstrated that static SIMS was very sensitive to the chemistry of molecular adsorbates on very carefully characterised single crystal metal surfaces.[1] Subsequently, the characterisation of the surface structure of organic materials has further confirmed and demonstrated this capability. To have real confidence in the technique an understanding of the fundamentals of the ion generation process is required. As indicated above and amplified in Chapters 6 to 9 there is now much evidence of growing understanding.

A detailed consideration of the procedures required for static SIMS spectral interpretation are discussed by Briggs in Chapter 16. Briefly, three spectral regions can be identified which provide information on the surface state of materials. There is what might be termed the *sub-monomer or fragment* region, that is in the *m/z* region below the pseudo molecular ion $M^{+/-}$ or if it is cationised $[M + C]^{+/-}$. Then there is the *n-mer* region where ions and fragments generated as a consequence of the bonding of two or three molecular (or monomer) units. Finally, for polymer type materials there is the *oligomer* spectral region usually generated via metal ion cationisation.

1.5.1 Sub-monomer or fragment region

This provides the fragmentation pattern spectrum which has been the main area of reference so far. Information on the basic chemical structure of the components of the material, the monomer(s) and any contamination should be accessible. This data is obtained by analysis of the fragmentation pattern. If the material being analysed is completely unknown this can really only be accomplished by comparing the major peaks in the spectrum with a library of standard spectra. Whilst enormous libraries are now available in conventional mass spectrometry, they are only just building for SSIMS.[37] Frequently, the methods of spectral interpretation are very similar to those used in conventional mass spectrometry although there are some significant differences. In positive-ion SSIMS *even electron* quasi-molecular ions are predominantly found, whereas in electron impact mass spectrometry (EI-MS) *odd electron* molecular ions are formed where a non-bonding electron is lost.

The other major difference is that negative-ion spectra are a very productive source of structural information in SSIMS, particularly for materials containing strongly electronegative heteroatoms, whereas negative ions are almost never found in EI-MS due to the inefficiency of electron attachment. The positive-ion spectrum is frequently cluttered with other hydrocarbon originating ions which do not of themselves seem very diagnostic. The negative-ion spectrum is free of these ions and hence when negative ions are formed they are frequently of significant diagnostic value. For example, the negative-ion spectra of the methacrylate polymers are far more informative than the positive.[38,39] The mechanism of ion formation seems to be much the same as that for positive ions, that is simple chain scission with unimolecular fragmentation processes. Since this region usually provides the most precise information on the chemical structure of the material, it is important that spectral assignment of the major peaks is accurate. Sometimes there are uncertainties where two or more possible ionic assignments have the same nominal mass.

This problem may be overcome by derivitisation or chemical labelling, by the use of MS/MS CAD techniques or by accurate mass measurement. The latter approach is only possible using a high mass resolution, $m/\Delta m > 4000$, ToF-SIMS instrument. Even this is not helpful if one wishes to identify the structure of a secondary ion species from a number of possibilities having the same stoichiometry. However, accurate mass measurement has been very helpful.

Recently it has been realised that, whilst there are peaks which are obviously diagnostic of particular surface chemistry, it is the *whole* spectrum which reflects the surface state. Some elements of the spectrum change more radically than others when the chemistry is modified, say in a plasma treatment. A weighting procedure is required to analyse the spectra. Multivariate statistical methods are being explored to enable static SIMS spectra of organic materials to be used define the surface chemistry in more detail.[40,41]

1.5.2 *n-mer* region

There are ions formed from a combination of a small number of monomer units or monomer units plus fragments. The exploration of the information content of this type of so-called *n-mer* ion suggests that they may contain valuable micro-structural information of the same type as from the fragmentation of the monomer units. However, they can also potentially provide more macromolecular information about the polymer structure. In copolymers the yield of *n-mers* composed of different combinations of the two components can indicate the extent, if any, of segregation.[42] For example, Gardella *et al.* have suggested that the statistical yield of *n-mers* of different lengths may point to folding or looping of a polymer chain at the surface.[43] There is also evidence that the cross-linking of polymers can be followed by changes in the yield of *n-mers* and even monomers. This would logically follow from the simple segmentation mechanism for sputtering.

1.5.3 Oligomer region

In the high mass region the most interesting ions are generated by the process of cationisation described by Hagenghoff in Chapter 11. Benninghoven and Hercules and co-workers have demonstrated that laying down a thin layer of an organic compound or polymer on a silver substrate and using the high mass range capability of ToF-SIMS it is possible to generate spectra of oligomer distributions $[M_x + Ag]^+$ to m/z >8000, Figure 10.[44,45] In principle, these spectra permit an estimate of the average molecular weight distributions to be determined. In some cases good agreement has been obtained with measurements from more conventional techniques such as gel permeation chromatography. However, the response of the channel plate detector can fall off with ion mass and care has to be taken in interpretation. Sample preparation is also crucial. The best results have been obtained when the polymer is laid down by evaporation or spin-casting to give a very thin patchy covering on silver. This removes charging problems and aids cationisation. This is not a possible arrangement for the analysis of thick polymer films or devices.

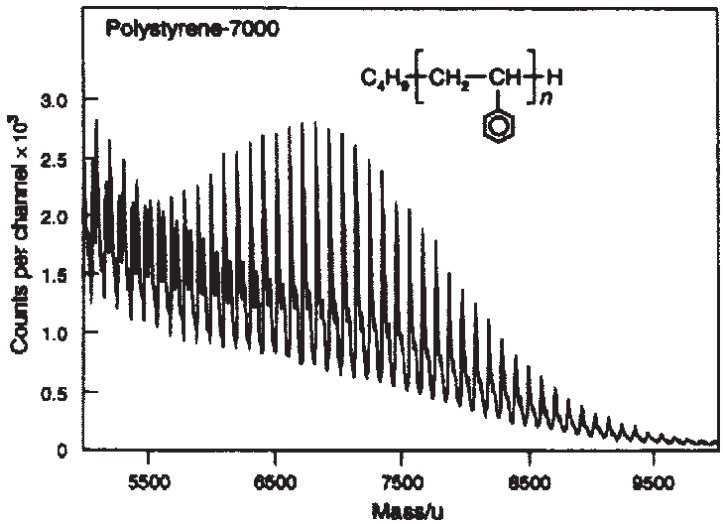

Figure 10. A cationised $[M_x + Ag]^+$ positive secondary ion spectrum of polystyrene 7000 on silver.

1.6 ToF-SIMS—What can it do?

A large proportion of this book is concerned with describing in considerable detail what ToF-SIMS can do in terms of practical surface chemical analysis. As Alfred Benninghoven says in his personal history (Chapter 2), he was instrumental in inventing a surprisingly versatile and powerful technique. Basically, its mass spectral capability provides powerful chemical specificity for even very complex materials. Combine this with the high spatial resolution capability of modern ion beams and we have a technique which can identify and locate surface chemistry with great precision and sensitivity. Chapters 18 to 28 describe in considerable detail many areas of real world surface technology where ToF-SIMS has made an important contribution. They range from polymer technology where ToF-SIMS has perhaps made its most significant impact, through areas of emerging importance in bio-sciences and bio-materials to environmental sciences, heterogeneous catalysis, the monitoring of contamination to the characterisation of photographic materials and ultra-shallow electronic devices.

Two examples from areas not so far covered by the book are particularly illustrative of the present strength and future potential of ToF-SIMS.[46,47]

1.6.1 Surface studies of wool fibres

Wool fibre is a complex natural material. The wool fibre consists of an inner cortex and an outer cuticle.[48] The cuticle itself is composed of an inner endocuticle, a "hard" highly cross-linked exocuticle and an outer hydrophobic epicuticle membrane. There is controversy over the existence of the epicuticle. Some believe it to be a resistant pro-

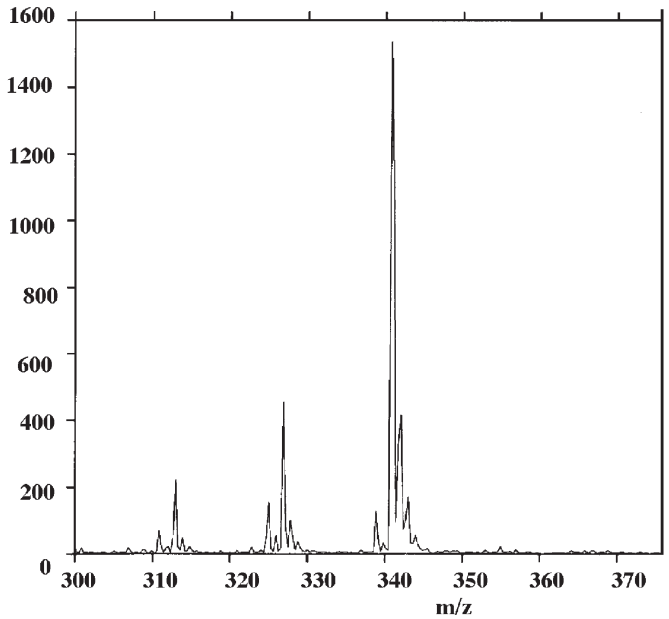

Figure 11. Negative-ion ToF-SIMS spectrum of clean mohair fibre. [Reproduced with permission from Volooj *et al.*, *Surf. Interface Anal.* 29, 422–431 (2000), © John Wiley & Sons Ltd].

tein/lipid membrane, 3–5 nm in thickness, whereas Höcker and co-workers suggest that the fatty acid lipids are directly bonded to the exocuticle.[49] However, it has been shown by wet chemical analysis that the major lipid component at the fibre surface is 18-methyleicosanoic acid (18-MEA), which is primarily, covalently bound to the protein via a thioester linkage:[50]

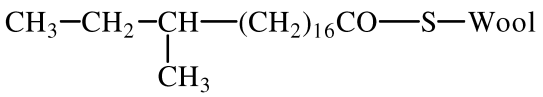

This conclusion was supported by early direct studies of the fibre surface by ToF-SIMS[51] which showed that some 70% of the surface fatty acids was 18-methyleicosanoic acid, the balance being made up of eicosanoic, stearic, oleic and palmitic acids.

Textile treatments which are directed towards improving the appearance can frequently adversely affect the feel and strength of the material. Bleaching processes are used to improve whiteness of pigmented wools. The traditional process attacked both the melanin to reduce the colour and also the keratin protein which reduced the strength of the fibre. A milder bleaching process has been developed incorporating an iron sulfate mordanting bath whose purpose is to enable a more selective catalysed peroxide bleaching of the melanin. Part of the negative ToF-SIMS spectrum of clean mohair fibre is

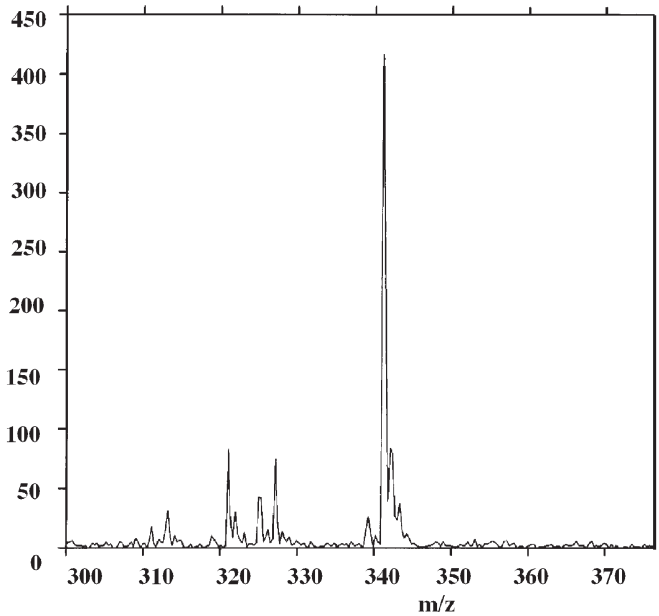

Figure 12. Negative-ion ToF-SIMS spectrum of scoured grey cashmere. [Reproduced with permission from Volooj *et al.*, *Surf. Interface Anal.* 29, 422–431 (2000), © John Wiley & Sons Ltd.]

shown in Figure 11. The major signal in this region at *m/z* 341 is due to 18 thioester linked MEA. Thioester linked eicosanoic acid is evident in much smaller concentration at *m/z* 327. At *m/z* 325 there is some evidence for small amounts of ester bonding of 18 MEA. The ToF-SIMS measurements suggest that relative surface concentration of 18 MEA in this fibre is about 50%, somewhat higher than the wet chemical analysis. Before bleaching, wool fibres are scoured using anionic surfactants. Although extensively rinsed these surfactants strongly adhere to the surface as evidenced by $C_{16}H_{33}OSO_3^-$ at *m/z* 321, Figure 12. Bleaching using the traditional method removes all the surface 18-MEA, Figure 13. The anionic surfactant is still very evident. This lipid loss manifests itself by greatly increased wetting and an obvious dry, harsh feel. The eicosanoic acid is relatively less affected. Previous ToF-SIMS studies of the effects of strong sunlight on wool fibre surfaces have shown that 18-MEA is the most sensitive of the surface lipids to photo-oxidation.[51] This sensitivity is mirrored here and may be a consequence of its location in the top surface.

The ToF-SIMS spectrum after the milder, more selective bleaching process shows that 18-MEA is still present on the surface although in lower concentration. The fibre is far less susceptible to wetting and has a better feel. Nevertheless the fibre has lost significant quantities of surface lipid, consequently its feel and wetting properties have been degraded. Protein hydrosolate conditioners have been developed whose purpose is to

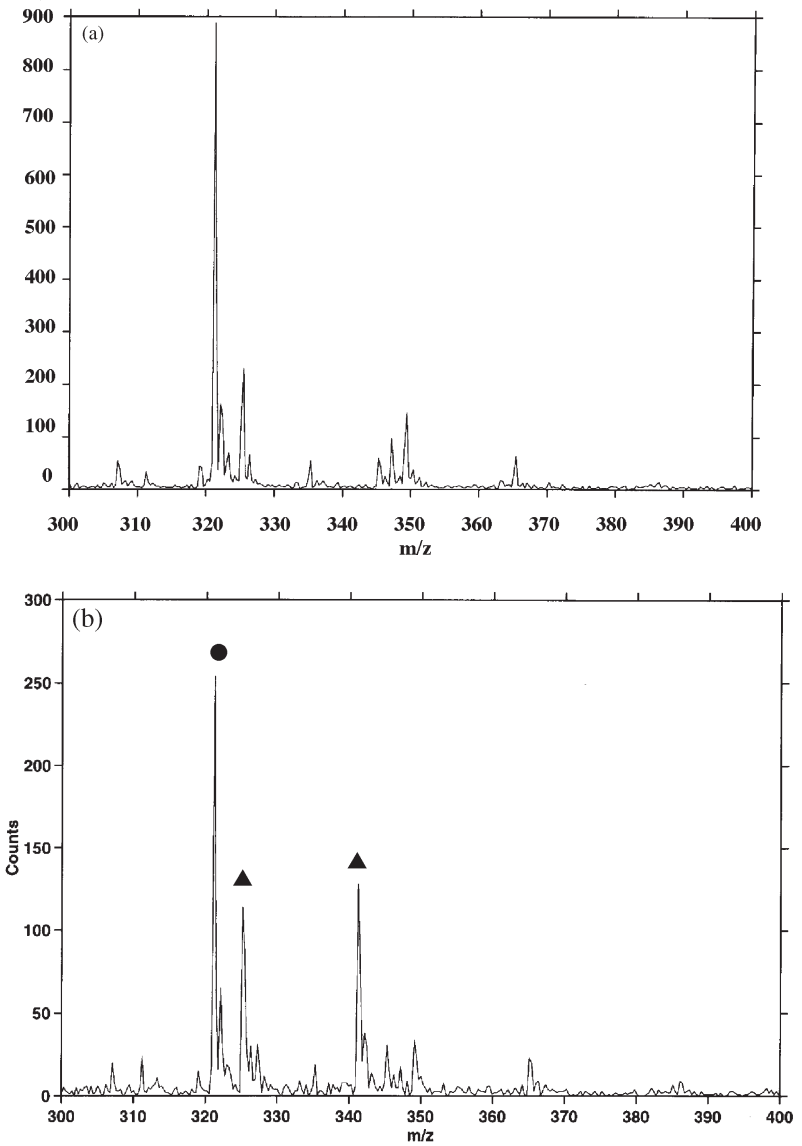

Figure 13. (a) Negative-ion ToF-SIMS spectrum of traditionally bleached cashmere fibres. (b) Negative-ion ToF-SIMS spectrum of selectively-bleached cashmere fibres. ▲ Surface lipid peaks; ● anionic surfactant residue. [Reproduced with permission from Volooj *et al.*, *Surf. Interface Anal.* 29, 422–431 (2000), © John Wiley & Sons Ltd.]

restore the fibre's softness (similar to hair conditioners!), for example, Apotex 1020 and Croquat WKPQS.[52] Apotex 1020 is a mixture of C_{10}, C_{12}, C_{14}, C_{16} and C_{18} alkyl protein derivatives with the typical structure:

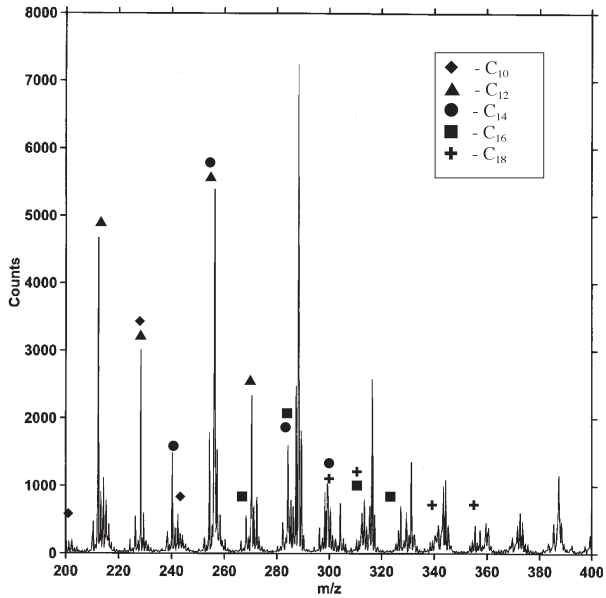

Figure 14. Positive-ion ToF-SIMS spectrum of Apotex 1020 alkyl protein softener film on aluminium. [Reproduced with permission from Volooj *et al.*, *Surf. Interface Anal.* 29, 422–431 (2000), © John Wiley & Sons Ltd.]

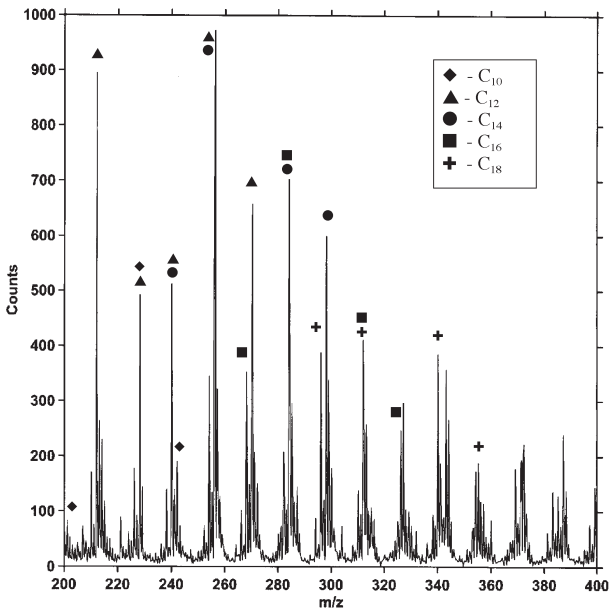

Figure 15. Positive-ion ToF-SIMS spectrum of selectively-bleached cashmere treated with 2% owf Apotex 1020 and hydroextracted. [Reproduced with permission from Volooj *et al.*, *Surf. Interface Anal.* 29, 422–431 (2000), © John Wiley & Sons Ltd.]

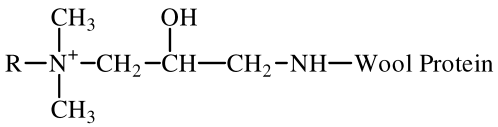

The Croquat WKPQS has the same structure, but with only the C_{14}, C_{16} and C_{18} derivatives present.

The spectra of these formulations are complex. Figure 14 shows the positive-ion spectrum of a thin film of Apotex 1020 on a metal foil. The complexity arises from complex ion fragmentation with spectral overlap of the constituent alkyl protein softeners. The principal peaks are quaternary ammonium ions and their fragments. Unravelling the spectrum involved obtaining spectra from one or two of the pure components. Each alkyl protein component does produce an unambiguous characteristic ion which allows semi-quantitative analysis of the components in the surface. Figure 15 shows the spectrum after the addition of Apotex 1020 to selectively bleached cashmere. It is immediately apparent that the surface of the cashmere is richer in C_{16} and C_{18} components than the pure Apotex film. It suggests that the fibre has a higher affinity for the more hydrophobic components. Quantitative assessment of the data confirms this impression. Although it is clear from the positive-ion spectrum that the surface has a high coverage of the conditioner, the negative-ion spectrum demonstrates that the coverage is non-uniform. The areas exposing the lipids and the anionic surfactant are not affected. Similar results showing the preferential adsorption of the C_{18} component were obtained for the Croquat formulation. This suggests a model for the functioning of the conditioner, namely that the cationic protein conditioner is tightly bound to the "exposed, damaged" oxidised anionic fibre surface protein, while the partially intact 18-MEA lipid layer prevents adsorption over itself by its hydrophobic nature. AFM studies of these conditioner treated surfaces seem to confirm this model. The selectively-bleached surfaces show non-uniformly distributed "globule" features, while the traditionally-bleached surfaces from which all 18-MEA had been removed exhibited a very much more uniform coating, Figure 16.

This is a powerful example of the degree to which ToF-SIMS is able to follow changes in surface chemistry as a complex material is processed.

1.6.2 ToF-SIMS—Chemical microscopy of biological material

Early in the development of static SIMS it was realised that if micro-focussed primary ion beams were used, particularly those based on liquid metal technology, the technique had the capability for high spatial resolution analysis. In the early- to mid-1980s a number of quadrupole-based SSIMS instruments were fitted with liquid gallium primary beams and 1 μm spatial resolution analysis became possible. Studies such as those from our own laboratory on the distribution of oxides at high temperature alloy surfaces and other similar applications (for example, mapping organic contaminants on semiconductor devices) illustrate the capability.[53] Such analysis places increased demands on sensitivity because the smaller the area analysed the smaller the number of atoms and molecules which can be removed for analysis and still maintain static conditions. To realise the

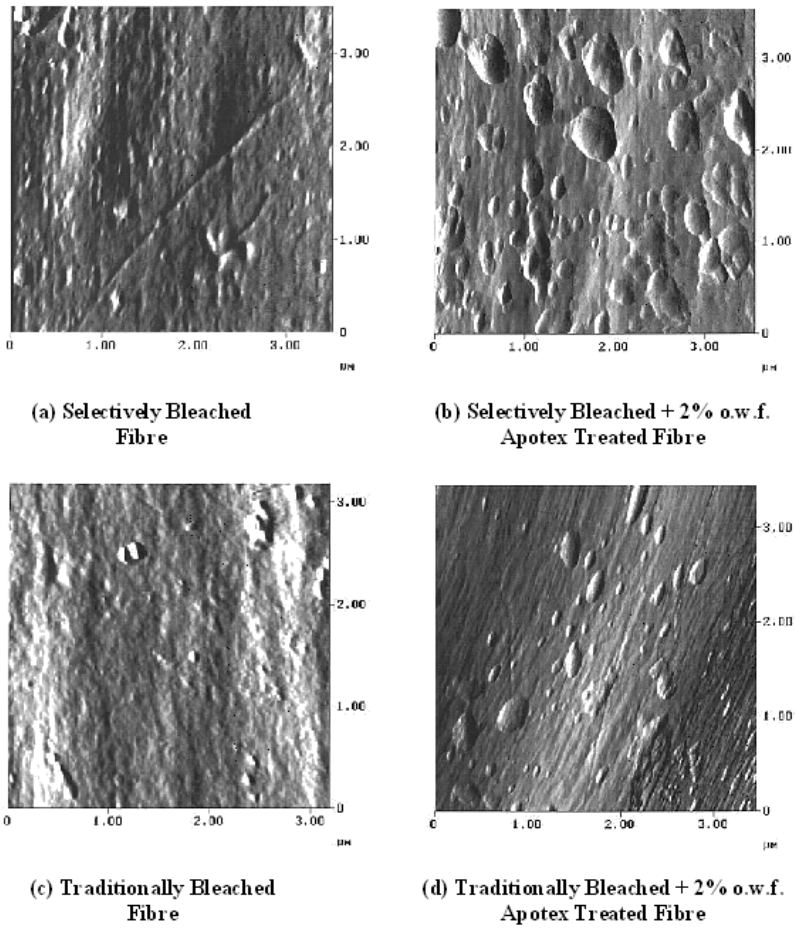

Figure 16. Atomic force microscopy images of traditionally- and selectively-bleached cashmere treated with Apotex 1020 protein softener protein. [Reproduced with permission from Volooj *et al.*, *Surf. Interface Anal.* 29, 422–431 (2000), © John Wiley & Sons Ltd.]

capability fully, as in other areas of SSIMS, the ToF-SIMS instrument was required. The first instrument configured specifically for imaging applications was commercialised by VG Ionics. It was based on the Poschenrieder geometry and was fitted with a 30 keV liquid gallium ion beam system. Sub-μm spatial resolution was possible with good sensitivity and moderate mass resolution.[54] Most ToF-SIMS instruments now have an imaging capability. Sub-100 nm resolution is attainable with high mass resolution and good sensitivity.

The spatial resolution capability combined with the chemical specificity of mass spectrometry suggests that ToF-SIMS should be capable of functioning as a chemical microscope (rather like and SEM with chemical sensitivity). Biology and the life-sci-

ences in general provide an enormous source of potential application areas for an instrument with such a capability. Clearly facilities such as freeze-fracture and precise low temperature control are required. The following example concerned with tobacco leaf chemistry shows the beginnings of what should be possible.

Stomata are tiny holes found mostly on the lower leaf surface whose purpose is to regulate plant respiration. Their main role is to allow CO_2 into the leaf for photosynthesis and waste O_2 to pass out. They are also the main site for water loss and therefore it is vital that plants have an effective mechanism for controlling the opening and closing of the stomata. This process is controlled by chemical changes in two surrounding guard cells. It is recognised that K^+ ions are important. As K^+ enters the guard cell, water follows by osmosis to make the guard cell turgid and the stomata open. Ca^{2+} ions are involved in intracellular signalling. They signal the movement of K^+, but high concentrations of Ca^{2+} should not enter the guard cells themselves otherwise they stay irreversibly shut. This spatially-distributed chemistry is shown in Figure 17. An ion-induced SEM image of an open stomata with its two surrounding guard cells can be seen in Figure 17(a) and in Figure 17(b) a combined K^+ and Ca^+ image shows a high concentration of K^+ (green) in the guard cells with a general distribution of Ca (blue) in the other surrounding cells.

Plants commonly respond to infection by "cell suicide", thereby establishing a region of dead tissue (a lesion) around a pathogenic microbe. This restricts the spread of the disease by limiting nutrient and water availability to the infecting microbes. In addition, the production of complex chemicals such as antibiotics is triggered in the surrounding living cells. The chemical effects of infection are shown in the sequence in Figure 18. The total ion image, which is equivalent to the physical image provided by an SEM, suggests an area of infection to the right of the image. The other three chemical images show that the living cells to the left have responded to the infection by increased concentrations of potassium and salicylic acid amongst other chemicals which have still to be identified. The lesion is particularly characterised by simple hydrocarbons characteristic of dead organic material. These materials have complex chemistry. Overlapping spectra result in complex spectra! Spectral interpretation can therefore be difficult. This is illustrated here. In addition to the elemental peaks which are easy to identify, the spectra from the leaf displays peaks at every mass channel. Related sequences can be identified but this may not immediately lead to definite molecular speciation. Good libraries of spectra covering all the compounds likely to be encountered are required. In this case a clear sequence of peaks was detected close to a lesion from *m/z* 169 down to *m/z* 43. Some peaks were separated by 14 mass units indicating the presence of CH_2 groups. There was some evidence of a CNO group, but as yet we have no library spectrum which identifies the compound. Figure 18(d).

These simple examples demonstrate the potential of ToF-SIMS for this type of study. They also throw up the complexities involved. The spectra show that the chemical composition of the living cells is far more complex than our account suggests. Identifying all the components will require the combination of a detailed spectral library of the possible cell components together with a search algorithm which is able to identify and sepa-

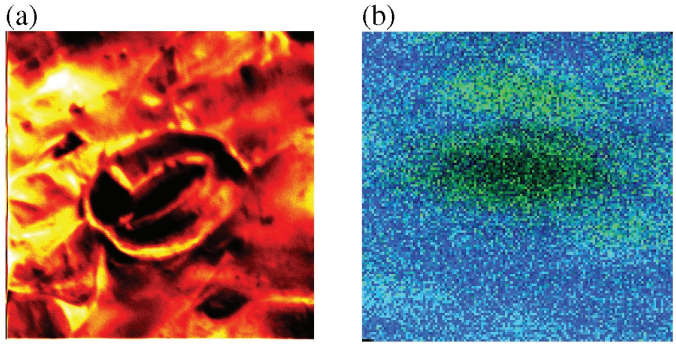

Figure 17. (a) Ion induced SEM of tobacco leaf stomata, 100 *μ*m field of view. (b) Potassium (green) over laid on a calcium (blue) image of tobacco leaf stomata, 75 *μ*m field of view. The potassium can be seen to be concentrated in the guard cells.

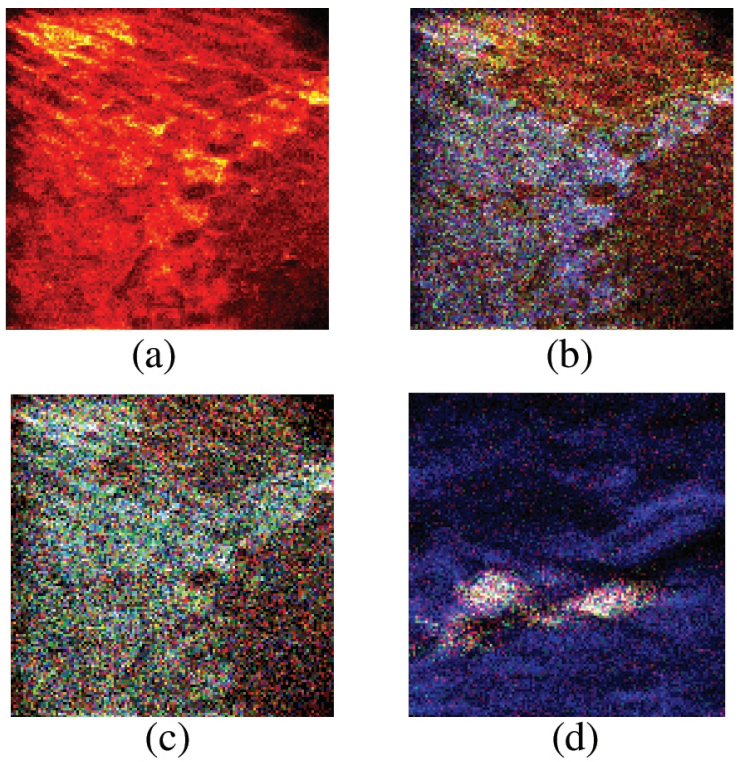

Figure 18. (a) Total positive-ion image of an area of infected tobacco leaf, field of view 600 *μ*m. The infected lesion is to the left of the image. (b) Overlaid positive-ion images of *m/z* 39 (blue) due to potassium and *m/z* 71 (green) due to salicylic acid in the healthy area and *m/z* 27 (red) due to C_2H_3 from hydrocarbon in the infected area. (c) Overlaid positive-ion images of *m/z* 15 (red) mainly in the infected area and *m/z* 71 and 85 (blue) in the healthy area. (d) An image of an unidentified molecular species comprising a sequence of related peaks from *m/z* 169 to *m/z* 43.

rate out the various components present and the application of advanced processing techniques of the type described by Tyler in Chapter 17. The Static SIMS Library is being assembled by the SSIMS community.[37] Search programmes are also being developed.[55] The prospects look good for ToF-SIMS to become a true chemical microscope if sensitivity issues can be fully addressed (see below).

1.7 What are the problem areas?

It will be clear from the above examples and many others through this book that ToF-SIMS has tremendous potential in terms of the enormous number of applications for high spatial resolution analysis of materials with complex chemistry. The possibilities in the life-sciences, biology and medicine are obvious, but the requirement to understand surface chemistry and interface interactions in almost all areas of high technology materials suggest that the need for static SIMS will be limitless. There are, however, three experimental issues which could limit its range of application unless solutions are found. They are alluded to in subsequent chapters, however, it is useful to summarise them here. They are all basically sensitivity issues.

1.7.1 Secondary ion yield limitations at high spatial resolution

It is clear that there is a limit to the spatial resolution which can be provided by SSIMS. The limit will be when the area probed is so small that there are too few molecules or atoms to provide an effective analysis. This issue is discussed in detail by Tyler in Chapter 17. Briefly, where that limit lies is a function of the detection limit of the technique as it is operated. The fundamental SIMS equation shows that the secondary ion yield is dependent on the sputter yield, Y, the ionisation probability, α, and the instrument transmission, η. The main limiting parameters are α which is generally $\leq 10^{-3}$ and η which using a ToF system maximises around 0.5. Thus if operation is restricted to the static limit of 10^{13} primary impacts cm^{-2}, (i.e. removal of no more than 10% of surface species) then Table 4 indicates that analysis at a pixel size smaller than 100 nm × 100 nm is not realistic since the *total* number of ions detected would be less than 20. If all these ions were distributed over a range of different chemical types, the signals would be lost in the noise.

The only solution is to increase secondary ion yield. There is the potential for an increase in yield of 10^3. There are two basic mechanisms by which this might be realised. One is to use the cationisation method referred to earlier (Hagenhoff, Chapter 11) and support the material of interest at high dilution on a silver substrate. Sputtering from such a substrate usually results in a high yield of silver cationised species of the type $[M + Ag]^+$. However, other than under a few favourable cases where it is possible to coat a surface partially with silver, this technique is not relevant to surface analysis.

The most effective way to increase ion yield is to post-ionise the vast number of neutral species emitted during sputtering (>95 % of the total yield) using laser generated photons, Figure 19. The geometry requires that a laser photon field intersects the sputtered neutral plume just above the sample surface. Three mechanisms are effective for

Table 4. Estimation of the number of molecules and atoms per pixel area as a function of pixel size.

Pixel size	Pixel area	Molecules per pixel[a]	Atoms per pixel
10 μm × 10 μm	10^{-6} cm^2	4×10^8	2.5×10^9
1 μm × 1 μm	10^{-8} cm^2	4×10^6	2.5×10^7
500 nm × 500 nm	2.5×10^{-9} cm^2	1×10^6	6.25×10^6
100 nm × 100 nm	1×10^{-10} cm^2	40,000	2.5×10^5
200 Å × 200 Å	4×10^{-12} cm^2	1600	10,000

[a]Assuming a molecular area of 5 Å × 5 Å

both elemental and molecular ionisation. They are described in some detail by Wucher, Pellin *et al*. and Lockyer in Chapters 13 to 15. In multi-photon resonant ionisation (REMPI) the wavelength of the photons are tuned to the energy levels which require to be traversed to enable the atom or molecule to be ionised. While the photon requirements

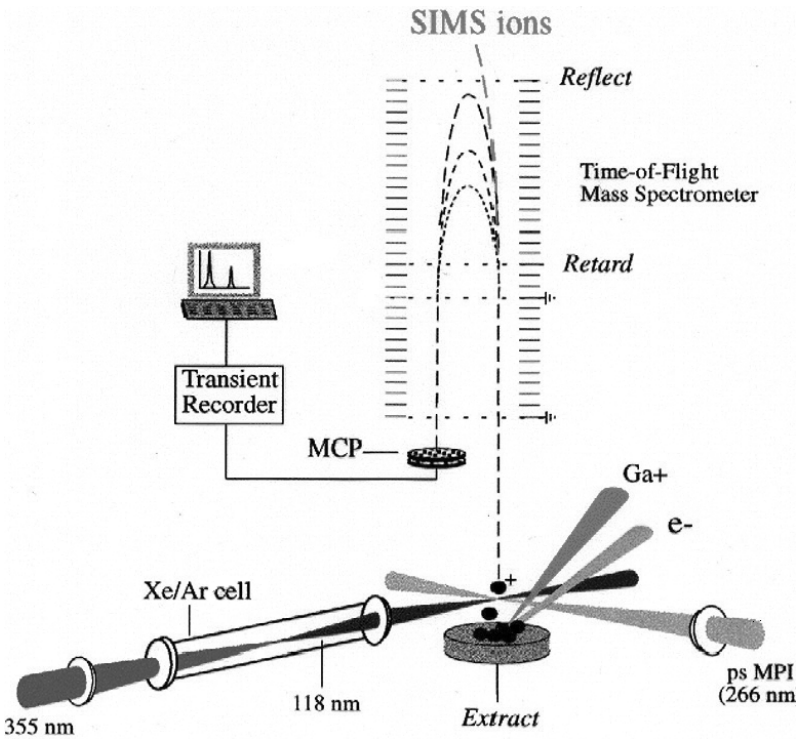

Figure 19. A schematic of the laser post-ionisation experiment.

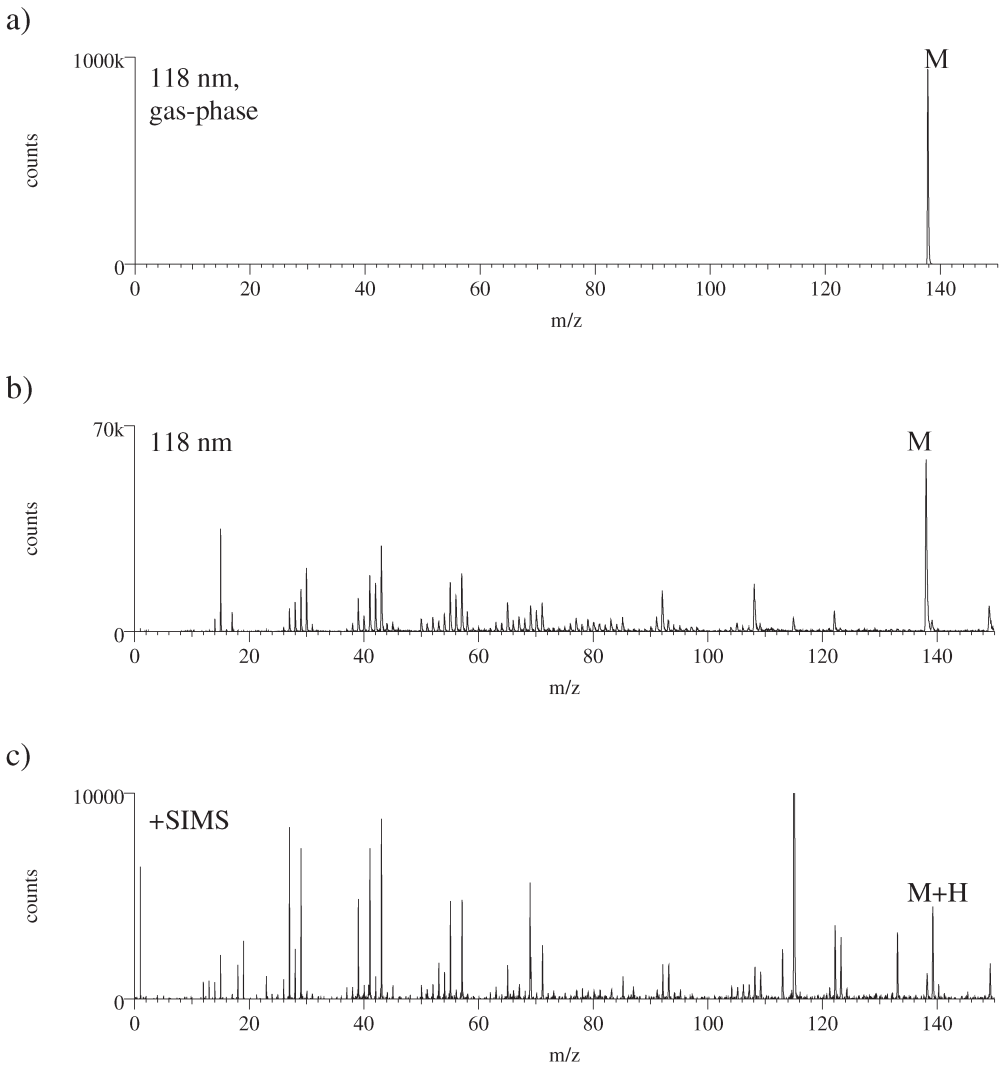

Figure 20. Positive-ion spectra of *p*-nitroaniline (a) 118 nm SPI of thermally-desorbed gas-phase molecules; (b) 118 nm SPI of sputtered neutral species; (c) ToF-SIMS. From Lockyer, Chapter 15.

can be quite specific, particularly for elemental ionisation, the process can be very efficient such that almost 100% ionisation can occur within the photon field. While very substantial increases in ion yield and hence sensitivity are accessible, it is clearly necessary to know what is being analysed so that the correct photon energies can be provided.

For unknown analysis non-resonant multiphoton ionisation (NRMPI) is used. Usually a single wavelength UV laser is used with very high power output such that the

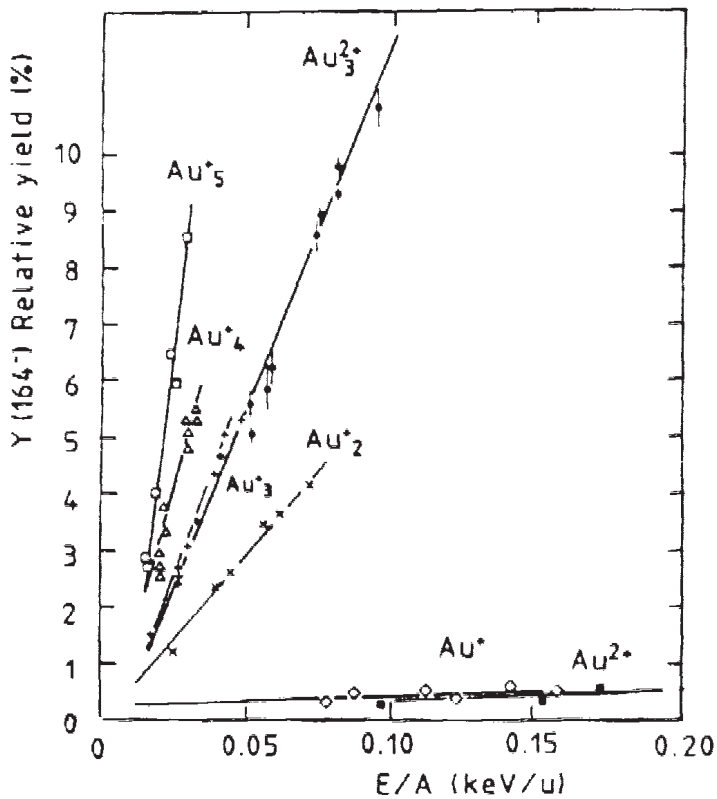

Figure 21. Yield variations of $[M - H]^-$ molecular ions (*m/z* 164) from a phenylalanine sample as a function of primary ion energy per mass unit (*E/A*). The primary ions are Au_n^{p+} with $n = 1$ to 5 and $p = 1$ or 2. [Reproduced with permission from M. Benguerba *et al.*, *Nucl. Instr. Meth., Phys. Res.* B62, 8 (1991).]

electron is ionised via virtual levels in the atom or molecule. This is less efficient than REMPI, but substantial increases in ion yield are possible with the result that high elemental yields are accessible. Unfortunately it is of no use for molecular ionisation because the high power results in multi-photon absorption and consequent over excitation and breakdown of the molecule. Single photon ionisation (SPI) is accomplished using VUV photons. The 157 nm VUV photons from the fluorine excimer laser enable species with ionisation potentials below 7.9 eV to be ionised, however, this is quite a restricted subset of molecular systems. By tripling the third harmonic 355 nm radiation from a Nd:YAG in a xenon/argon gas mixture, 118 nm photons with energy of 10.5 eV are provided.[56] The power is low, but since no more than a single photon absorption is optimum, this is an advantage. This is a relatively new field and the database of compounds and materials studied is small, however, the initial results suggest a significant improvement in ion yield for a number of compounds, see Lockyer in Chapter 15.

1.7.2 Molecular fragmentation of sputtered molecule

Although post-ionisation is potentially capable of increasing the secondary ion yield substantially, the resulting REMPI and SPI spectra from sputtered organic materials reveal substantially more low mass fragmentation compared to similar spectra obtained from the same materials thermally desorbed into the gas phase, Figure 20. It is clear that sputtered molecules are desorbed with large amounts of vibrational internal energy, which when augmented by further photon energy can result in rather extensive fragmentation with the loss of some of the most chemically characteristic ions, namely the large molecular or monomer ions. This is behaviour is predicted in the molecular dynamics sputtering models described by Garrison in Chapter 9. The kinetic energy distributions measured by Delcorte *et al.* also demonstrate this phenomenon, Chapter 7. Some method is required to either cool the sputtered species after emission or we need a "cooler" sputtering method.

1.7.3 Ion yields for high mass molecular species

A related "problem" is that compared to MALDI, the SIMS process does not release really high mass species (>1000–10,000 Da) with high yield. The MALDI process is thought to proceed by an explosive emission of lots of material at once. In static SIMS we do not want to remove large quantities of material and what we do remove we want to come off gently! It has been suggested that the use of polyatomic primary ions could be advantageous in this regard. Because the primary ion energy is partitioned amongst many components each individual impact would be gentler, but spread out more. Most of the energy would be delivered nearer the surface to generate a "splash". Perhaps this would enable larger molecules to be removed from the surface. In the early1990s Le Beyec and co-workers observed that Au_n^+ cluster ions delivered large non-linear increases in the secondary ion yield of admittedly small molecular ions—phenylalanine, Figure 21.[57] Benninghoven's group has shown that SF_5^+ primary ions deliver significant increases in high mass yields.[58] Very recent work in the UMIST group has demonstrated that a 10 keV C_{60}^+ beam can deliver very considerable increases in secondary ion yield. In the case of gramicidin D the increase in the molecular ion yield compared to a gallium ion beam was over 5000, Figure 22. In Chapter 12, von Stipdonk describes the current state of experimentation in this area. It is clear that higher yields of high mass species can be detected using polyatomic ions, however, there is also some suggestion of higher fragment or rearranged ion yields. Molecular dynamics modelling suggests that large molecular species require multiple cooperative sputtering impacts in order to be released from the surface intact,[59] see Chapter 9. Increased fragmentation may result as a consequence of multiple direct impact on different parts of a large molecular species by components of the primary particle, or because although the sputtering occurs via lower energy processes, because there are more of them, there is a net increase in internal energy.

Both the use of laser post-ionisation and polyatomic primary beams holds promise of significant improvements in chemically significant ion yields. However, considerable

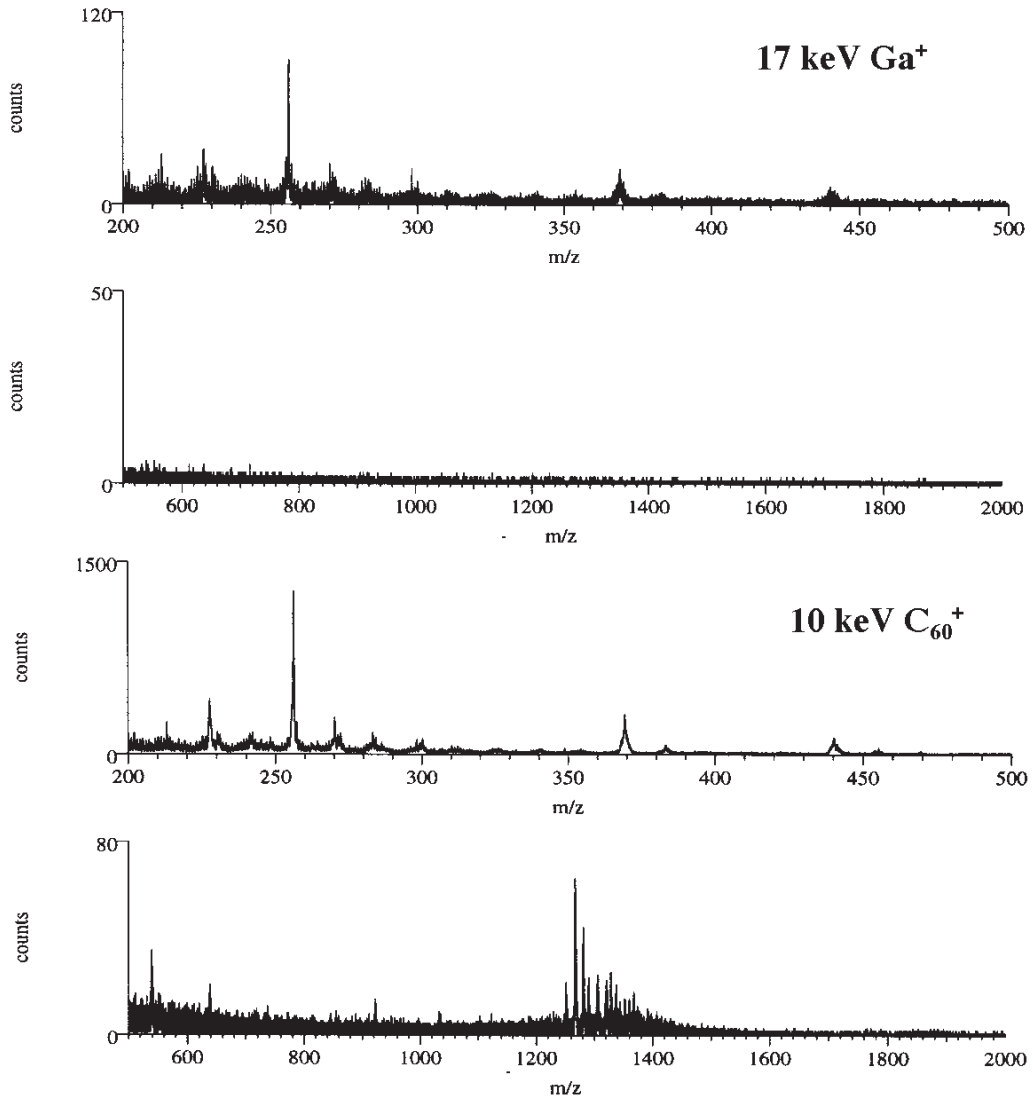

Figure 22. Part of the positive-ion SSIMS spectrum from a thick layer of gramicidin-D, upper spectrum obtained with a 17 keV gallium ion beam; the lower spectrum with 10 keV C_{60} ion beam. The gallium dose was 10 times the C_{60} dose.

research is still required to clarify many of the uncertain issues which surround them before we can be sure of the increased ion yields which would deliver a reliable and robust chemical microscope at the spatial resolution levels which would enable ToF-SIMS to realise its potential fully.

1.8 References

1. M. Barber, J.C. Vickerman and J. Wolstenholme, *JCS Faraday I* **72,** 40 (1976) and subsequent papers reviewed in J.C. Vickerman, *Surf. Sci.* **189/190,** 7 (1987).
2. J.C. Vickerman, A. Brown and N.M. Reed (Eds), *Secondary Ion Mass Spectrometry, Principles and Applications*. Oxford University Press (1989).
3. D. Briggs, A. Brown and J.C. Vickerman (Eds), *Handbook of Static SIMS.* John Wiley & Sons Ltd, Chichester, UK (1989).
4. (a) R. Behrisch (Ed.), *Sputtering by Particle Bombardment, I*, Springer Series Topics in Applied Physics Volume 47. Springer Verlag, Berlin, Germany (1981); (b) R. Behrisch (Ed.), *Sputtering by Particle Bombardment, II*, Springer Series Topics in Applied Physics, Volume 52. Springer Verlag, Berlin, Heidelberg, Germany (1983); (c) R. Behrisch and K. Wittmaack (Eds), *Sputtering by Particle Bombardment, III*, Springer Series Topics in Applied Physics, Volume 64. Springer Verlag, Berlin, Germany (1991).
5. A. Benninghoven, F. Rüdenauer and W. Werner, *Secondary Ion Mass Spectrometry*. John Wiley & Sons Ltd, Chichester, UK (1987).
6. W. Sicthermann and A. Benninghoven, *Int. J. Mass Spectrom. Ion Phys.* **40,** 177 (1981).
7. I.S. Gilmore and M.P. Seah, *Surf. Interface Anal.* **24,** 746 (1996).
8. R. Galera, J. Blais and G. Bolbach, *Int. J. Mass Spectrom. Ion Proc.* **107,** 531 (1991).
9. A. Benninghoven, in *Ion Formation from Organic Solids (IFOS III)*, Springer Series in Chemical Physics, Volume 25, Ed by A. Benninghoven. Springer Verlag, Berlin, Germany, p. 64 (1983).
10. D. Briggs and M.J. Hearn, *Int. J. Mass Spectrom. Ion Processes* **67,** 47 (1985).
11 (a) D. Briggs and M.J. Hearn, *Vacuum* **36,** 1005 (1986); (b) G.J. Leggett and J.C. Vickerman, *Anal. Chem.* **63,** 561 (1991); (c) G.J. Leggett and J.C. Vickerman, *Appl. Surf. Sci.* **55,** 105 (1992).
12. N.M. Reed, P. Humphrey and J.C. Vickerman, in *Secondary Ion Mass Spectrometry, SIMS VII*, Ed by A. Benninghoven, C.A. Evans, K.D. McKeegan, H.A. Storms and H.W. Werner. J. Wiley & Sons Ltd, Chichester, UK, p. 809 (1990); (b) A. Brown and J.C. Vickerman, *Surf. Interface Anal.* **8,** 75 (1986).
13. D. Surman, J.A. van den Berg and J.C. Vickerman, *Surf. Interface Anal.* **4,** 160 (1982).
14. (a) D. Greifendorf, P. Beckmann, M. Schemmer and A. Benninghoven, in *Ion Formation from Organic Solids (IFOSIII)*, Ed by A. Benninghoven, Springer Series in Chemical Physics Volume 25. Springer Verlag, Berlin, Germany, p. 118 (1983); (b) D. Rading, R. Kersting and A. Benninghoven, in *Secondary Ion Mass Spectrometry, SIMS XI*, Ed by G. Gillen, R. Lareau, J. Bennett and F. Stevie. John Wiley & Sons, Chichester, UK, p. 455 (1998).
15. M.J. Hearn and D. Briggs, *Surf. Interface Anal.* **11,** 198 (1988).

16. (a) G.J. Leggett and J.C. Vickerman, *Int. J. Mass Spectrom. Ion Phys.* **122,** 281 (1992); (b) G.J. Leggett and J.C. Vickerman, *Ann Rep. Roy. Soc. Chem., C* 77 (1991).
17. (a) A. Delcorte and P. Bertrand, *Nucl. Instrum. Meth. Phys. Res. B* **117,** 235 (1996); (b) A. Delcorte and P. Bertrand, *Nucl. Instr. and Meth. B* **135,** 430 (1998); (c) A. Delcorte and P. Bertrand, *Surf. Sci.* **412/413,** 97 (1998).
18. D. Rading, R. Kersting and A. Benninghoven, *J. Vac. Sci. Tchnol. A* **18,** 312 (2000).
19. G. Leggett, in *The Static SIMS Library,* Ed by J.C. Vickerman, D. Briggs and A. Henderson, SurfaceSpectra Ltd, Manchester, UK (1999).
20. R.M. Braun, P. Blenkinsopp, S.J. Mullock, C. Corlett, K.F. Willey, J.C. Vickerman and N. Winograd. *Rapid Commun. Mass Spectrom.* **12,** 1246 (1998).
21. Ionoptika Ltd, www.ionoptika.com.
22. (a) A. Müller and A. Benninghoven, *Surf. Sci.* **39,** 427 (1973); (b) C. Plog, L. Wiederman and A. Benninghoven, *Surf. Sci.* **67,** 565 (1977); (c) M. Barber, J.C. Vickerman and J. Wolstenholme, *JCS Faraday I* **72,** 40 (1976); (d) *Surf. Sci.* **68,** 130 (1977); (e) D. Briggs, A. Brown and J.C. Vickerman (Eds), *Handbook of Static SIMS*. John Wiley & Sons Ltd, Chichester, UK (1989).
23. B.T. Chait and K.G. Standing, *Int. J. Mass Spectrom. Ion Phys.* **40,** 185 (1981).
24. K. Tang, R. Bevis, W. Ens, F. Lafortune, B. Schueler and K.G. Standing, *Int. J. Mass Spectrom. Ion Proc.* **85,** 43 (1988); E. Niehuis, T. Heller, F. Feld and A. Benninghoven, *J. Vac. Sci. Technol.* **A5,** 1243 (1987); A.J. Eccles and J.C. Vickerman, *J. Vac. Sci. Technol.* **A7,** 234 (1989).
25. Kore R-500, Kore Ltd, www.kore.co.uk.
26. P. Sigmund, in *Sputtering by Particle Bombardment, Part I*, Ed by R. Behrisch, Springer Series Topics in Applied Physics, Volume 47. Springer Verlag, Berlin, Germany, p. 9 (1981).
27. N. Winograd, *Prog. Solid State Chem.* **13,** 285 (1981).
28. N. Winograd, *Mat. Fys. Medd. Dan. Vid. Selsk.* **43,** 223 (1993).
29. (a) A. Wucher and B.J. Garrison, *Surf. Sci.* **260,** 257 (1992); (b) A. Wucher and B.J. Garrison, *Phys. Rev.* **B46,** 4855 (1992).
30. K.S.S. Liu, C.W. Yong, B.J. Garrison and J.C. Vickerman, *J. Phys. Chem. B* **103,** 3195 (1999).
31 A. Delcorte, X. Vanden Eynde, P. Bertrand, J.C. Vickerman and B.J. Garrison, *J. Phys. Chem. B* **104,** 2673 (2000).
32. W. Gerhard and C. Plog, *Z. Phys. B, Cond. Matt.* **54,** 59 and 71 (1989).
33. C. Plog, L. Wiedermann and A. Benninghoven, *Surf. Sci.* **67,** 565 (1977).
34. R.T. Sanderson, in *Solid State Chemistry and its Applications,* Ed by A.R. West. Wiley, Chichester, p. 291 (1987).
35. N.M. Reed and J.C. Vickerman, in *Practical Surface Analysis, Vol. 2, Ion and Neutral Spectroscopy*, Ed by D. Briggs and M.P. Seah. John Wiley & Sons, Chichester, UK, p. 332 (1992).
36. R.G. Cooks and K.L. Busch, *Int. J. Mass Spectrom. Ion Phys.* **53,** 111 (1983).

37. J.C. Vickerman, D. Briggs and A. Henderson, *The Static SIMS Library*. SurfaceSpectra Ltd, Manchester, UK (1998).
38. A. Brown and J.C. Vickerman, *Surf. Interface Anal.* **8,** 75 (1986).
39. D. Briggs and M.A. Hearn, *Surf. Interface Anal.* **11,** 198 (1988).
40. A. Chilkoti, B.D. Ratner and D. Briggs, in *Secondary Ion Mass Spectrometry, SIMS VIII*, Ed by A. Benninghoven, K.T.F. Janssen, J. Tümpner and H.W. Werner. John Wiley & Sons Ltd, Chichester, UK, p. 815 (1992).
41. B. Tyler, A. Willse, Hong Shi and R.E. Peterson, in *Secondary Ion Mass Spectrometry, SIMS XII*, Ed by A. Benninghoven, P. Bertrand, H.N. Migeon and H.W. Werner. Elsevier, Amsterdam, The Netherlands, p. 943 (2000).
42. J. Lub, F.C.B.M. van Vroonhoven, D. van Leyen and A. Benninghoven, *J. Polym. Sci. A, Polym Chem.* **27,** 4035 (1989).
43. K.J. Hook, T.J. Hook, J.H. Wandass and J.A. Gardella, Jr, *Appl. Surf. Sci.* **44,** 29 (1990).
44. D. van Leyen, M. Deimel, B. Hagenhoff and A. Benninghoven, in *Secondary Ion Mass Spectrometry, SIMS VII*, Ed by A. Benninghoven, C.A. Evans, K.D. McKeegan, H.A. Storms and H.W. Werner. John Wiley & Sons Ltd, Chichester, UK, p. 757 (1990).
45. I.V. Blestos, D.M. Hercules, D. van Leyen, B. Hagenhoff, E. Niehius and A. Benninghoven, *Anal. Chem.* **63,** 1953 (1991).
46. S.J. Vooloij, C.M. Carr, R. Mitchell and J.C. Vickerman, *Surf. Interface Anal.* **29,** 422 (2000).
47. J. Burns, L.P. Lockyer and J.C. Vickerman, unpublished data.
48. J.A. Maclaren and B. Milligan, "Wool Science", *The Chemical Reactivity of the Wool Fibre*. Science Press, Marricksville, Australia (1981).
49. K.H. Phan, H. Thomas and E. Heine, *Proc. Int. Wool. Res. Conf., Biella,* Vol II, p. 19 (1995).
50. (a) A.P. Negri, H.J. Cornell and D.E. Rivett, *Text. Res. J.* **63,** 109 (1993); (b) D.J. Peet, R.E.M. Wettenhall and D.E. Rivett, *Text. Res. J.* **65,** 58 (1995).
51. D.C. Jones, C.M. Carr, W.D. Cooke, R. Mitchell and J.C. Vickerman, *Proc. Int. Wool Text. Res. Conf., Biella*, Vol. IV, p. 245 (1995).
52. Brookstone and Croda Chemicals.
53. (a) D.G. Lees, P. Rowland, A. Brown and J.C. Vickerman, in *Handbook of Static SIMS*, Ed vy D. Briggs, A. Brown and J.C. Vickerman. John Wiley & Sons Ltd, Chichester, UK, p. 148 (1989); (b) A. Brown and J.C. Vickerman, *Surf. Interface Anal.* **9,** 309 (1986); (c) A. Brown, A.J. Eccles, J.A. van den Berg and J.C. Vickerman, *Secondary Ion Mass Spectrometry, SIMS V*, (Washington DC 1985), Springer Verlag Series in Chemical Physics, Volume 44. Springer Verlag, Berlin, Germany, pp. 257–260 (1986).
54. (a) D. Briggs and M.J. Hearn, *Surf. Interface Anal.* **13,** 181 (1988); (b) A.J. Eccles and J.C. Vickerman, *J. Vac. Sci. Technol.* **A7,** 234 (1989).

55. O.D. Sanni, A. Henderson and J.C. Vickerman, in *Secondary Ion Mass Spectrometry, SIMS XII*, Ed by A. Benninghoven, P. Bertrand, H.N. Migeon and H.W. Werner. Elsevier, Amsterdam, The Netherlands, p. 805 (2000).
56. N.P. Lockyer and J.C. Vickerman, *Laser Chem.* **17,** 139 (1997).
57. M. Benguerba, A. Brunelle, S. Della-Negra, J. Depauw, H. Joret, Y. Le Beyec, M.G. Blain, E.A. Schweikert, G. Ben Assayag and P. Sudraund, *Nucl. Instr. Meth., Phys. Res.* **B62,** 8 (1991); Y. Le Beyec, *Int. J. Mass Spectrom. Ion Proc.* **174,** 101 (1998).
58. B. Hagenhoff, P.L. Cobben, C. Bendel, E. Niehius and A. Benninghoven, in *Secondary Ion Mass Spectrometry, SIMS XI*, Ed by G. Gellen, R. Lareau, J. Bennett and F. Stevie. John Wiley & Sons Ltd, Chichester, UK, p. 585 (1998).
59. A. Delcorte, X. Vanden Eynde, P. Bertrand, J.C. Vickerman and B.J. Garrison, *J. Phys Chem. B* **104,** 2673 (2000).